MODELING AND SIMULATION OF PERMANENT MAGNET SYNCHRONOUS MOTOR DRIVE SYSTEM

by

Enrique L. Carrillo Arroyo

A thesis submitted in partial fulfillment of the requirements for the degree of

MASTER OF SCIENCE
in
ELECTRICAL ENGINEERING

UNIVERSITY OF PUERTO RICO
MAYAGÜEZ CAMPUS
2006

Approved by:

_____   _____
Carlos Cuadros, PhD   Date
Member, Graduate Committee

_____   _____
Efrain O'Neill-Carrillo, PhD   Date
Member, Graduate Committee

_____   _____
Krishnaswami Venkatesan, PhD   Date
President, Graduate Committee

_____   _____
Andrés Calderón, PhD   Date
Representative of Graduate Studies

_____   _____
Isidoro Couvertier, PhD   Date
Chairperson of the Department

ABSTRACT

The thesis deals with the detailed modeling of a permanent magnet synchronous motor drive system in Simulink. Field oriented control is used for the operation of the drive. The simulation includes all realistic components of the system. This enables the calculation of currents and voltages in different parts of the inverter and motor under transient and steady conditions. The losses in different parts are calculated, facilitating the design of the inverter.

A closed loop control system with a Proportional Integral (PI) controller in the speed loop has been designed to operate in constant torque and flux weakening regions. Implementation has been done in Simulink. A comparative study of hysteresis and Pulse Width Modulation (PWM) control schemes associated with current controllers has been made in terms of harmonic spectrum and total harmonic distortion. Simulation results are given for two speeds of operation, one below rated and another above rated speed.

RESUMEN

Este trabajo trata de modelaje detallado de motores sincrónicos de imán permanente en sistemas de mando utilizando Simulink. La simulación incluye todos los componentes reales del sistema de mando, permitiendo el cálculo de corrientes y voltajes en las diferentes partes del inversor y el del motor durante condiciones transitorias y en estacionarias. Las perdidas en las diferentes partes son calculadas para facilitar el diseño del inversor.

Un sistema de lazo cerrado con un controlador PI en el lazo de velocidad fue diseñado para operar en las regiones de torque constante y reducción de flujo. Se realizo la implementación utilizando Simulink. Un estudio comparativo de los métodos de control hysteresis y PWM asociados a controladores de corriente, en términos de espectro harmónico y total de distorsión harmónica. Resultados de las simulaciones son presentadas para dos velocidades de operación, uno bajo la velocidad de placa y otra sobre la velocidad de placa.

To my family . . .

ACKNOWLEDGEMENTS

During my graduate studies in the University of Puerto Rico several persons collaborated directly and indirectly with my research. Without their support it would be impossible for me to finish my work. That is why I wish to dedicate this section to recognize their support.

I want to start expressing a sincere acknowledgement to my advisor, Dr. Krishnaswami Venkatesan because he gave me the opportunity to research under his guidance and supervision. I received motivation; encouragement and support from him during my studies and for the completion of my work. I also want to express my gratitude to Dr. Carlos Cuadros and Dr. Efraín O'Neill-Carrillo for serving as member of my graduate committee, for reviewing of the thesis and for their valuable advice during the course of the master's program. This work was supported in part by the Center of Power Electronics Systems (CPES) as well as by the University of Puerto Rico-Mayagüez.

At last, but the most important I would like to thank my family, for their unconditional support, inspiration and love.

TABLE OF CONTENTS

TABLE LIST

FIGURE LIST

Symbols

B	friction
BDCM	Brushless DC Motor
CSI	Current Source Inverter
d	Direct o polar axis
f_c	crossover frequency
i_a, i_b, i_c	Three phase currents
i_d	d-axis current
i_f	equivalent permanent magnet field current
i_q	q-axis current
I_m	Peak value of supply current
IGBT	Insolate Gate Bipolar Transistor
IPM	Interior Permanent Magnet
J	inertia
L	self inductance
L_d	d-axis self inductance
L_{ls}	stator leakage inductance
L_{dm}	d-axis magnetizing inductance
L_{qm}	q-axis magnetizing inductance
L_q	q-axis self inductance
L_s	equivalent self inductance per phase

P	number of poles
PI	proportional integral
PM	Permanent Magnet
PMSM	Permanent Magnet Synchronous Motor
q	Quadrature or interpolar axis
Rs	stator resistance
SPM	Surface Permanent Magnet
Te	develop torque
TL	load torque
V_a, V_b, V_c	Three phase voltage
V_d	d-axis voltage
V_q	q-axis voltage
VSI	Voltage Source Inverter
ρ	derivative operator
λ_d	flux linkage due d axis
λ_f	PM flux linkage or Field flux linkage
λ_q	flux linkage due q axis
θ_r	rotor position
ω_m	rotor speed
ω_r	electrical speed
ω_{rated}	motor rated speed

1 INTRODUCTION

Permanent magnet (PM) synchronous motors are widely used in low and mid power applications such as computer peripheral equipments, robotics, adjustable speed drives and electric vehicles.

The growth in the market of PM motor drives has demanded the need of simulation tools capable of handling motor drive simulations. Simulations have helped the process of developing new systems including motor drives, by reducing cost and time. Simulation tools have the capabilities of performing dynamic simulations of motor drives in a visual environment so as to facilitate the development of new systems.

In this work, the simulation of a field oriented controlled PM motor drive system is developed using Simulink. The simulation circuit will include all realistic components of the drive system. This enables the calculation of currents and voltages in different parts of the inverter and motor under transient and steady conditions. The losses in different parts can be calculated facilitating the design of the inverter.

A closed loop control system with a PI controller in the speed loop has been designed to operate in constant torque and flux weakening regions. Implementation has been done in Simulink. A comparative study of hysteresis and PWM control schemes associated with current controllers has been made in terms of harmonic spectrum and total harmonic distortion. Simulation results are given for two speeds of operation, one below rated and another above rated speed.

1.1 Motivation

Modeling and simulation is usually used in designing PM drives compared to building system prototypes because of the cost. Having selected all components, the simulation process can start to calculate steady state and dynamic performance and losses that would have been obtained if the drive were actually constructed. This practice reduces time, cost of building prototypes and ensures that requirements are achieved.

In works available until now ideal components have been assumed in the inverter feeding the motor and simulations have been carried out. The voltages and currents in different parts of the inverter have not been obtained and hence the losses and efficiency can not be calculated. In this work, the simulation of a PM motor drive system is developed using Simulink. The simulation circuit includes all realistic components of the drive system. This enables the calculation of currents and voltages in different parts of the inverter and motor under transient and steady conditions. The losses in different parts are calculated. A comparative study associated with hysteresis and PWM control techniques in current controllers has been made.

A speed controller has also been designed for closed loop operation of the drive. Design method for the PI controller is also given.

1.2 Previous Work

PM motor drives have been a topic of interest for the last twenty years. Different authors have carried out modeling and simulation of such drives.

In 1986 Sebastian, T., Slemon, G. R. and Rahman, M. A. [1] reviewed permanent magnet synchronous motor advancements and presented equivalent electric circuit models for such motors and compared computed parameters with measured parameters. Experimental results on laboratory motors were also given.

In 1986 Jahns, T.M., Kliman, G.B. and Neumann, T.W. [2] discussed that interior permanent magnet (IPM) synchronous motors possessed special features for adjustable speed operation which distinguished them from other classes of ac machines. They were robust high power density machines capable of operating at high motor and inverter efficiencies over wide speed ranges, including considerable range of constant power operation. The magnet cost was minimized by the low magnet weight requirements of the IPM design. The impact of the buried magnet configuration on the motor's electromagnetic characteristics was discussed. The rotor magnetic saliency preferentially increased the quadrature-axis inductance and introduced a reluctance torque term into the IPM motor's torque equation. The electrical excitation requirements for the IPM synchronous motor were also discussed. The control of the sinusoidal phase currents in magnitude and phase angle with respect to the rotor orientation provided a means for achieving smooth responsive torque control. A basic feed forward algorithm for executing this type of current vector torque control was discussed, including the implications of current regulator saturation at high speeds. The key results were illustrated using a combination of simulation and prototype IPM drive measurements.

In 1988 Pillay and Krishnan, R. [3], presented PM motor drives and classified them into two types such as permanent magnet synchronous motor drives (PMSM) and brushless dc motor (BDCM) drives. The PMSM has a sinusoidal back emf and requires sinusoidal stator currents to produce constant torque while the BDCM has a trapezoidal back emf and requires rectangular stator currents to produce constant torque. The PMSM is very similar to the wound rotor synchronous machine except that the PMSM that is used for servo applications tends not to have any damper windings and excitation is provided by a permanent magnet instead of a field winding. Hence the d, q model of the PMSM can be derived from the well known model of the synchronous machine with the equations of the damper windings and field current dynamics removed. Equations of the PMSM are derived in rotor reference frame and the equivalent circuit is presented without dampers. The damper windings are not considered because the motor is designed to operate in a drive system with field-oriented control. Because of the nonsinusoidal variation of the mutual inductances between the stator and rotor in the BDCM, it is also shown in this paper that no particular advantage exists in transforming the abc equations of the BCDM to the d, q frame.

As an extension of his previous work, Pillay, P. and Krishnan, R. in 1989 [4] presented the permanent magnet synchronous motor (PMSM) which was one of several types of permanent magnet ac motor drives available in the drives industry. The motor had a sinusoidal flux distribution. The application of vector control as well as complete modeling, simulation, and analysis of the drive system were given. State space models of the motor and speed controller and real time models of the inverter switches and vector controller were included. The machine model was derived for the PMSM from the wound rotor synchronous

motor. All the equations were derived in rotor reference frame and the equivalent circuit was presented without dampers. The damper windings were not considered because the motor was designed to operate in a drive system with field-oriented control. Performance differences due to the use of pulse width modulation (PWM) and hysteresis current controllers were examined. Particular attention was paid to the motor torque pulsations and speed response and experimental verification of the drive performance were given.

Morimoto, S., Tong, Y., Takeda, Y. and Hirasa, T. in 1994 [5], in their paper aimed to improve efficiency in permanent magnet (PM) synchronous motor drives. The controllable electrical loss which consisted of the copper loss and the iron loss could be minimized by the optimal control of the armature current vector. The control algorithm of current vector minimizing the electrical loss was proposed and the optimal current vector could be decided according to the operating speed and the load conditions. The proposed control algorithm was applied to the experimental PM motor drive system, in which one digital signal processor was employed to execute the control algorithms, and several drive tests were carried out. The operating characteristics controlled by the loss minimization control algorithm were examined in detail by computer simulations and experimental results.

The paper in 1997 by Wijenayake, A.H. and Schmidt, P.B. [6], described the development of a two-axis circuit model for permanent magnet synchronous motor (PMSM) by taking machine magnetic parameter variations and core loss into account. The circuit model was applied to both surface mounted magnet and interior permanent magnet rotor configurations. A method for on-line parameter identification scheme based on no-load parameters and saturation level, to improve the model, was discussed in detail. Test schemes

6

to measure the equivalent circuit parameters, and to calculate saturation constants which govern the parameter variations were also presented.

In 1997 Jang-Mok, K. and Seung-Ki, S. [7], proposed a novel flux-weakening scheme for an Interior Permanent Magnet Synchronous Motor (IPMSM). It was implemented based on the output of the synchronous PI current regulator reference voltage to PWM inverter. The on-set of flux weakening and the level of the flux were adjusted inherently by the outer voltage regulation loop to prevent the saturation of the current regulator. Attractive features of this flux weakening scheme included no dependency on the machine parameters, the guarantee of current regulation at any operating condition, and smooth and fast transition into and out of the flux weakening mode. Experimental results at various operating conditions including the case of detuned parameters were presented to verify the feasibility of the proposed control scheme.

Bose, B. K., in 2001 [8], presented different types of synchronous motors and compared them to induction motors. The modeling of PM motor was derived form the model of salient pole synchronous motor. All the equations were derived in synchronously rotating reference frame and was presented in the matrix form. The equivalent circuit was presented with damper windings and the permanent magnet was represented as a constant current source. Some discussions on vector control using voltage fed inverter were given.

Bowen, C., Jihua, Z. and Zhang, R. in 2001 [9], addressed the modeling and simulation of permanent magnet synchronous motor supplied from a six step continuous inverter based on state space method. The motor model was derived in the stationary reference frame and then in the rotor reference frame using Park transformation. The

simulation results obtained showed that the method used for deciding initial conditions was very effective.

In 2002 Mademlis, C. and Margaris, N. [10], presented an efficiency optimization method for vector-controlled interior permanent-magnet synchronous motor drive. Based on theoretical analysis, a loss minimization condition that determines the optimal q-axis component of the armature current was derived. Selected experimental results were presented to validate the effectiveness of the proposed control method.

In 2004, Jian-Xin, X., Panda, S. K., Ya-Jun, P., Tong Heng, L. and Lam, B. H. [11] applied a modular control approach to a permanent-magnet synchronous motor (PMSM) speed control. Based on the functioning of the individual module, the modular approach enabled the powerfully intelligent and robust control modules to easily replace any existing module which did not perform well, meanwhile retaining other existing modules which were still effective. Property analysis was first conducted for the existing function modules in a conventional PMSM control system: proportional-integral (PI) speed control module, reference current-generating module, and PI current control module. Next, it was shown that the conventional PMSM controller was not able to reject the torque pulsation which was the main hurdle when PMSM was used as a high-performance servo. By virtue of the internal model, to nullify the torque pulsation it was imperative to incorporate an internal model in the feed-through path. This was achieved by replacing the reference current-generating module with an iterative learning control (ILC) module. The ILC module records the cyclic torque and reference current signals over one entire cycle, and then uses those signals to update the reference current for the next cycle. As a consequence, the torque pulsation could

be reduced significantly. In order to estimate the torque ripples which might exceed certain bandwidth of a torque transducer, a novel torque estimation module using a gain-shaped sliding-mode observer was further developed to facilitate the implementation of torque learning control. The proposed control system was evaluated through real-time implementation and experimental results validated the effectiveness.

Araujo, R.E., Leite, A.V. and Freitas, D.S. in 1997 [12], mentioned the different simulation tools available and the benefits that were obtained by accelerating the process for the development of visual design concepts. Among various software packages for simulation of electronic circuits, like SPICE and SABER, EMTP, EUROSTAG, or for specialized simulations tools for power electronics system like SIMPLORER, POSTMAC, SIMSEN, ANSIM, and PSCAD, they had chosen MATLAB/Simulink. MATLAB/Simulink had user-friendly environment, visual design, Real-Time Workshop and libraries of models for the various components of a power electronic system.

Ong, C in 1998 [13], explained the need for powerful computation tools to solve complex models of motor drives. Among the different simulation tools available for dynamic simulation he had chosen MATLAB/SIMULINK® as the platform for his book because of the short learning curve required to start using it, its wide distribution, and its general purpose nature.

Macbahi, H. Ba-razzouk, A. Xu, J. Cheriti, A. and Rajagopalan, V. in 2000 [14], mentioned that a great number of universities and researchers used the MATLAB/SIMULINK software in the field of electrical machines because of its advantages

such as   user friendly environment, visual oriented programming concept, non-linear standard blocks and a large number of toolboxes for special applications.

In 1997 Reece, J.H., Bray, C.W., Van Tol, J.J. and Lim, P.K. [15], discussed three possible computer simulation tools such as PSpice, HARMFLO and the Electromagnetic Transients Program (EMTP) in their project on power systems containing adjustable speed drives. They selected EMTP as the primary simulation tool because of its broad range of capabilities, which were well matched to their problem.

French, C.D., Finch, J.W. and Acarnley, P.P. in 1998 [16], had found that in recent years the increase in desktop computing power has lead to an increase in the sophistication of both design and simulation tools available to the design engineer. One such tool becoming more wide spread amongst academia and industry was Mathwork's Simulink / Matlab package. This paper described how Simulink could be used as an integrated development environment for simulation and real time control of electric motor drive systems. This was carried out with the aid of motor models together with simulation and real time control circuits. It was demonstrated how such a set-up could be used as a cost effective control system rapid prototyping scheme.

Onoda, S. and Emadi, A. in 2004 [17], had developed a modeling tool to study automotive systems using the power electronics simulator (PSIM) software. PSIM was originally made for simulating power electronic converters and motor drives. This user-friendly simulation package was able to simulate electric/electronic circuits.

Venkaterama, G. [18]; had developed a simulation for permanent magnet motors using Matlab/simulink. The motor was a 5 hp PM synchronous line start type. Its model included the damper windings required to start the motor and the mathematical model was derived in rotor reference frame. The simulation was presented with the plots of rotor currents, stator currents, speed and torque.

Simulink PM Synchronous Motor Drive demo circuit (2005) [19] used the AC6 block of SimPowerSystems library. It modeled a permanent magnet synchronous motor drive with a braking chopper. The PM synchronous motor was fed by a PWM voltage source inverter, which was built using a Universal Bridge Block. The speed control loop used a PI regulator to produce the flux and torque references for the vector control block. The vector control block computed the three reference motor line currents corresponding to the flux and torque references and then fed the motor with these currents using a three-phase current regulator. Motor current, speed, and torque signals were available at the output of the block.

The demo circuit (2005) in Simulink for Permanent magnet synchronous motor fed by PWM inverter [20] had a three-phase motor rated 1.1 kW, 220 V, 3000 rpm. The PWM inverter was built entirely with standard Simulink blocks. Its output went through Controlled Voltage Source blocks before being applied to the PMSM block's stator windings. Two control loops were used. The inner loop regulated the motor's stator currents. The outer loop controlled the motor's speed. Line to line voltages, three phase currents, speed and torque were available at the output of the scope blocks.

In the above works, none of them have considered a real drive system simulation in Simulink operating at constant torque and flux weakening regions.

1.3 Outline of the Present Work

The thesis is divided into 6 chapters. Chapter 2 presents a theoretical review of permanent magnet motors drives which includes permanent magnet materials, classification of the permanent magnet motors, position sensors, inverters and current controllers. Chapter 3 deals with the detailed modeling of PMSM, closed loop control techniques used for PM motor drives, field oriented control of the motor in constant torque and flux-weakening regions, and the design of speed control for PM motor. The fourth chapter is dedicated to the simulation. It deals with the selection of the simulation tool for dynamic simulation of motor drives. The real drive system is simulated using Simulink with block by block explanation. Chapter 5 deals with the simulation results. A comparative study of PMW and Hysteresis current controllers used with this drive system has been made in terms of total harmonic distortion. Finally, Chapter 6 presents general conclusions and recommendations for future work.

2 DESCRIPTION OF THE DRIVE SYSTEM

This chapter deals with the description of the different components such as permanent magnet motors, position sensors, inverters and current controllers of the drive system. A review of permanent magnet materials and classification of permanent magnet motors is also given.

2.1 Permanent Magnet Synchronous Motor Drive System

The motor drive consists of four main components, the PM motor, inverter, control unit and the position sensor. The components are connected as shown in figure 2.1.
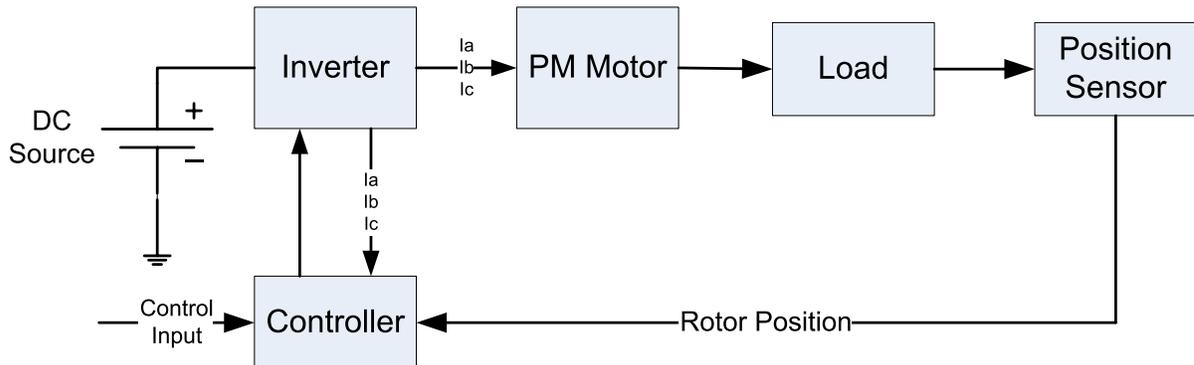

Figure 2.1 Drive System Schematic

Descriptions of the different components are as follows:

2.2 Permanent Magnet Synchronous Motor

A permanent magnet synchronous motor (PMSM) is a motor that uses permanent magnets to produce the air gap magnetic field rather than using electromagnets. These motors have significant advantages, attracting the interest of researchers and industry for use in many applications.

2.2.1 Permanent Magnet Materials

The properties of the permanent magnet material will affect directly the performance of the motor and proper knowledge is required for the selection of the materials and for understanding PM motors.

The earliest manufactured magnet materials were hardened steel. Magnets made from steel were easily magnetized. However, they could hold very low energy and it was easy to demagnetize. In recent years other magnet materials such as Aluminum Nickel and Cobalt alloys (ALNICO), Strontium Ferrite or Barium Ferrite (Ferrite), Samarium Cobalt (First generation rare earth magnet) (SmCo) and Neodymium Iron-Boron (Second generation rare earth magnet) (NdFeB) have been developed and used for making permanent magnets.

The rare earth magnets are categorized into two classes: Samarium Cobalt (SmCo) magnets and Neodymium Iron Boride (NdFeB) magnets. SmCo magnets have higher flux density levels but they are very expensive. NdFeB magnets are the most common rare earth magnets used in motors these days. A flux density versus magnetizing field for these magnets is illustrated in figure 2.2.
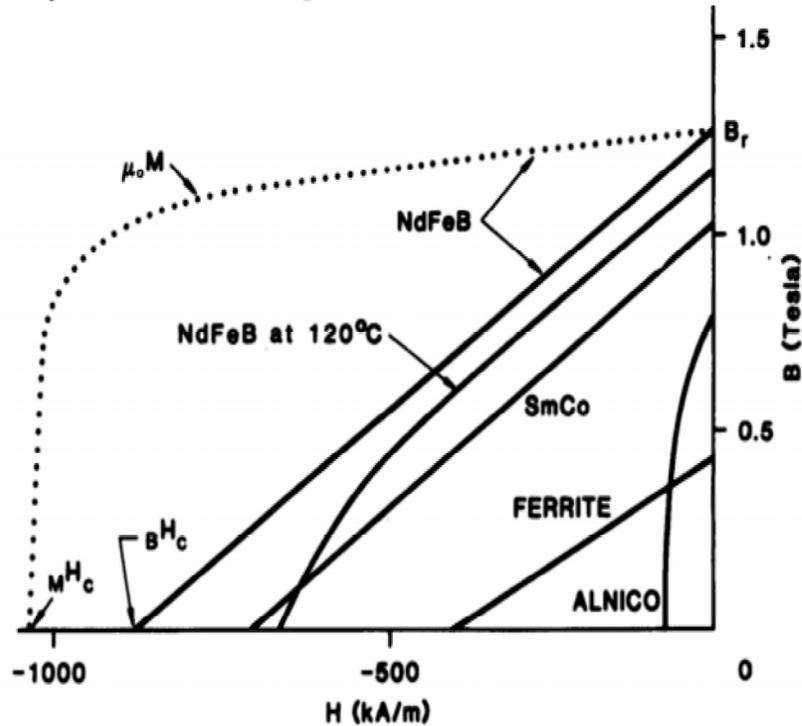
Figure 2.2 Flux Density versus Magnetizing Field of Permanent Magnetic Materials[21]

2.2.2 Classification of Permanent Magnet Motors

2.2.2.1 Direction of field flux

PM motors are broadly classified by the direction of the field flux. The first field flux classification is radial field motor meaning that the flux is along the radius of the motor. The second is axial field motor meaning that the flux is perpendicular to the radius of the motor. Radial field flux is most commonly used in motors and axial field flux have become a topic of interest for study and used in a few applications.

2.2.2.2   Flux density distribution

PM motors are classified on the basis of the flux density distribution and the shape of current excitation. They are PMSM and PM brushless motors (BLDC). The PMSM has a sinusoidal-shaped back EMF and is designed to develop sinusoidal back EMF waveforms. They have the following:

1.   Sinusoidal distribution of magnet flux in the air gap

2.   Sinusoidal current waveforms

3.   Sinusoidal distribution of stator conductors.

BLDC has a trapezoidal-shaped back EMF and is designed to develop trapezoidal back EMF waveforms. They have the following:

1.   Rectangular distribution of magnet flux in the air gap

2.   Rectangular current waveform

3.   Concentrated stator windings.

2.2.2.3   Permanent magnet radial field motors

In PM motors, the magnets can be placed in two different ways on the rotor. Depending on the placement they are called either as surface permanent magnet motor or interior permanent magnet motor.

Surface mounted PM motors have a surface mounted permanent magnet rotor. Each of the PM is mounted on the surface of the rotor, making it easy to build, and specially skewed poles are easily magnetized on this surface mounted type to minimize cogging torque. This configuration is used for low speed applications because of the limitation that the

magnets will fly apart during high-speed operations. These motors are considered to have small saliency, thus having practically equal inductances in both axes [22]. The permeability of the permanent magnet is almost that of the air, thus the magnetic material becoming an extension of the air gap. For a surface permanent magnet motor $L_d = L_q$ [8].

The rotor has an iron core that may be solid or may be made of punched laminations for simplicity in manufacturing [23]. Thin permanent magnets are mounted on the surface of this core using adhesives. Alternating magnets of the opposite magnetization direction produce radially directed flux density across the air gap. This flux density then reacts with currents in windings placed in slots on the inner surface of the stator to produce torque. Figure 2.3 shows the placement of the magnet.
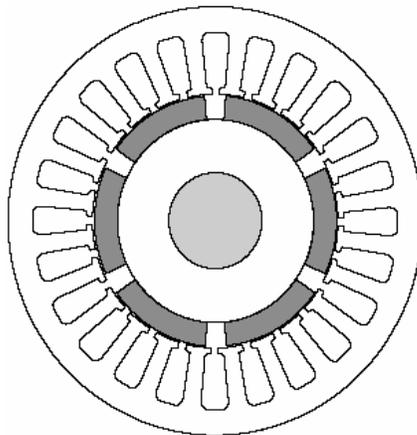

Figure 2.3 Surface Permanent Magnet Motor [21]

Interior PM motors have interior mounted permanent magnet rotor as shown in figure 2.4. Each permanent magnet is mounted inside the rotor. It is not as common as the surface-mounted type but it is a good candidate for high-speed operation. There is inductance variation for this type of rotor because the permanent magnet part is equivalent to air in the

magnetic circuit calculation. These motors are considered to have saliency with q axis inductance greater than the d axis inductance ($L_q > L_d$)[8].
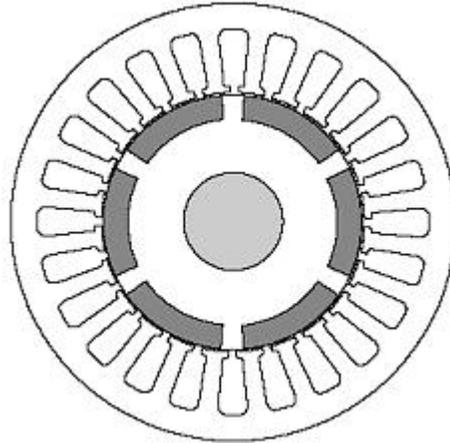

Figure 2.4 Interior Permanent Magnet Motor [21]

2.3 Position Sensor

Operation of permanent magnet synchronous motors requires position sensors in the rotor shaft when operated without damper winding. The need of knowing the rotor position requires the development of devices for position measurement. There are four main devices for the measurement of position, the potentiometer, linear variable differential transformer, optical encoder and resolvers. The ones most commonly used for motors are encoders and revolvers. Depending on the application and performance desired by the motor a position sensor with the required accuracy can be selected

2.3.1 Optical Encoders

The most popular type of encoder is the optical encoder as shown in figure 2.5, which consists of a rotating disk, a light source, and a photo detector (light sensor). The disk, is mounted on the rotating shaft, has coded patterns of opaque and transparent sectors. As the disk rotates, these patterns interrupt the light emitted onto the photo detector, generating a digital pulse or output signal.
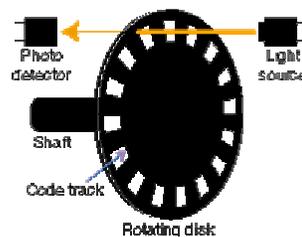

Figure 2.5 Optical Encoder [24]

Optical encoders offer the advantages of digital interface. There are two types of optical encoders, incremental encoder and absolute encoder.

2.3.1.1   Incremental encoders

Incremental encoders have good precision and are simple to implement but they suffer from lack of information when the motor is at rest position and in order for precise position the motor most be stop at the starting point.

The most common type of incremental encoder uses two output channels (A and B) to sense position. Using two code tracks with sectors positioned 90° degrees out of phase, the two output channels of the quadrature encoder indicate both position and direction of rotation as shown in figure 2.6. If A leads B, for example, the disk is rotating in a clockwise direction. If B leads A, then the disk is rotating in a counter-clockwise direction. By monitoring both,

19

the number of pulses and the relative phase of signals A and B, it's possible to track position and direction of rotation. Some quadrature encoders also include a third output channel, called a zero or index or reference signal, which supplies a single pulse per revolution. This single pulse is used for precise determination of a reference position. The precision of the encoder is fix by its code disk but it can be increased by detecting the Up and Down transitions on both the A and B channels.
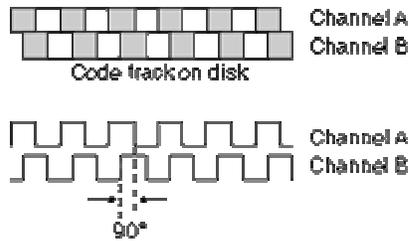

Figure 2.6 Quadrature Encoder Channels [25]

2.3.1.2   Absolute encoders

The absolute encoder, as shown in figure 2.7 captures the exact position of the rotor with a precision directly related to the number of bits of the encoder. It can rotate indefinitely and even if the motor stops the position can be measured or obtained.

It provides a "whole word" output with a unique code pattern representing each position. This code is derived from independent tracks on the encoder disc (one for each "bit" of resolution) corresponding to individual photo detectors. The output from these detectors is HI (light) or LO (dark) depending on the code disc pattern for that particular position.
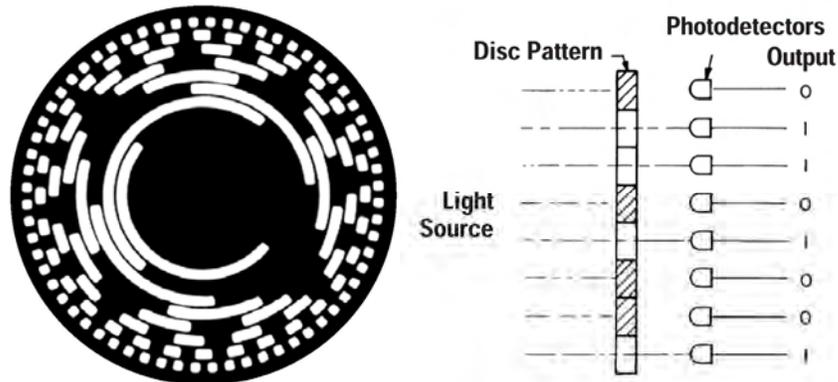
Figure 2.7 Absolute Encoder [26]

Absolute encoders are used in applications where a device is inactive for long periods of time or moves at a slow rate, such as flood gate control, telescopes, cranes, valves, etc. They are also recommended in systems that must retain position information through a power outage.

2.3.2 Position Revolver

Position revolver as shown in figure 2.8, also called rotary transformers, works on the transformer principle. The primary winding is placed on the rotor and depending upon the rotor shaft angle the induced voltage at the two secondary windings of the transformer shifted by 90° would be different. The position can be calculated using the two voltages.

The resolver is basically a rotary transformer with one rotating reference winding (V_{ref}) and two stator windings. The reference winding is fixed on the rotor, and therefore, it rotates jointly with the shaft passing the output windings, as is depicted in figure 2.8. Two stator windings are placed in quadrature (shifted by 90°) with one another and generate the sine and cosine voltages (V_{sin}, V_{cos}) respectively. Both windings will be further referred to as

output windings. In consequence of the excitement applied on the reference winding Vref and along with the angular movement of the motor shaft θ, the respective voltages are generated by resolver output windings V_{sin} , V_{cos}.
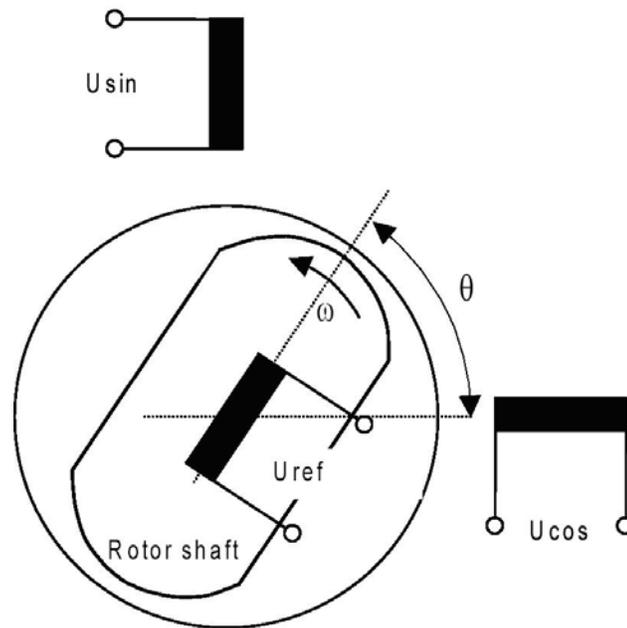

Figure 2.8 Resolver [27]

The frequency of the generated voltages is identical to the reference voltage and their amplitudes vary according to the sine and cosine of the shaft angle θ. Considering that one of the output windings is aligned with the reference winding, then it is generated full voltage on that output winding and zero voltage on the other output winding and vice versa. The rotor angle θ can be extracted from these voltages shown in figure 2.9.
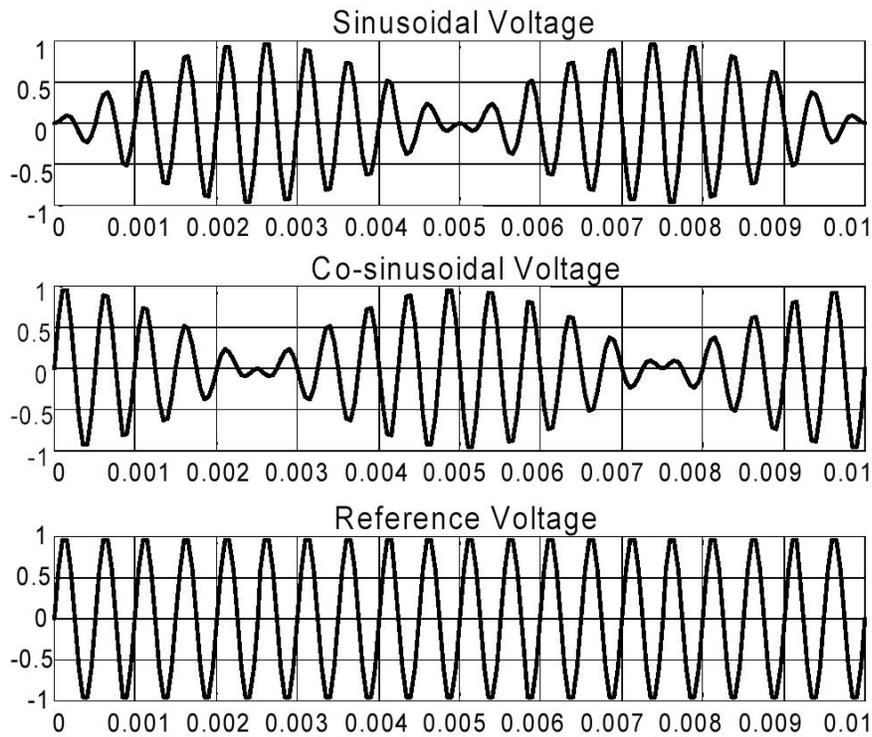
Figure 2.9 Excitation and Output Signal of the Resolver [27]

The shaft angle can be determined by an Inverse Tangent [8] function of the quotient of the sampled resolver output voltages $V_{\sin}$, $V_{\cos}$. This determination can be expressed, in terms of resolver output voltages, as follows:

$$\theta = a\tan(\frac{U\sin}{U\cos})$$

2.4 Current Controlled Inverter

The motor is fed form a voltage source inverter with current control. The control is performed by regulating the flow of current through the stator of the motor. Current controllers are used to generate gate signals for the inverter. Proper selection of the inverter devices and selection of the control technique will guarantee the efficacy of the drive.

2.4.1 Inverter

Voltage Source Inverters are devices that convert a DC voltage to AC voltage of variable frequency and magnitude. They are very commonly used in adjustable speed drives and are characterized by a well defined switched voltage wave form in the terminals [23]. Figure 2.10 shows a voltage source inverter. The AC voltage frequency can be variable or constant depending on the application.
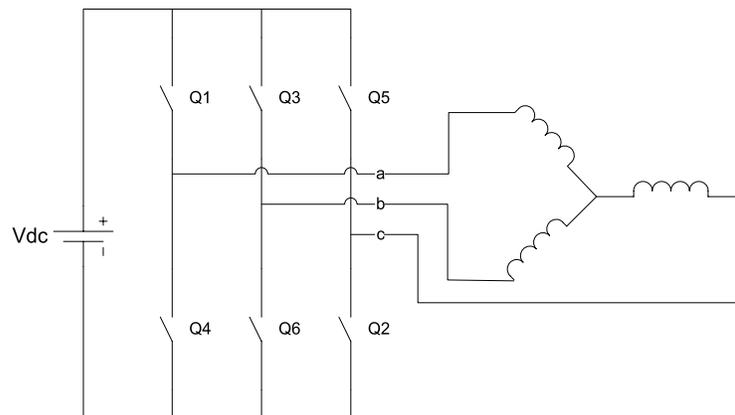

Figure 2.10 Voltage Source Inverter Connected to a Motor

Three phase inverters consist of six power switches connected as shown in figure 2.10 to a DC voltage source. The inverter switches must be carefully selected based on the requirements of operation, ratings and the application. There are several devices available

today and these are thyristors, bipolar junction transistors (BJTs), MOS field effect transistors (MOSFETs), insulated gate bipolar transistors (IGBTs) and gate turn off thyristors (GTOs). The devices list with their respective power switching capabilities are shown in table 2.1 MOSFETs and IGBTs are preferred by industry because of the MOS gating permits high power gain and control advantages. While MOSFET is considered a universal power device for low power and low voltage applications, IGBT has wide acceptance for motor drives and other application in the low and medium power range. The power devices when used in motor drives applications require an inductive motor current path provided by antiparallel diodes when the switch is turned off. Inverters with antiparallel diodes are shown in figure 2.11.

Table 2.1 Devices Power and Switching Capabilities

| Device	Power Capability	Switching Speed
BJT	Medium	Medium
GTO	High	Low
IGBT	Medium	Medium
MOSFET	Low	High
THYRISTOR	High	Low
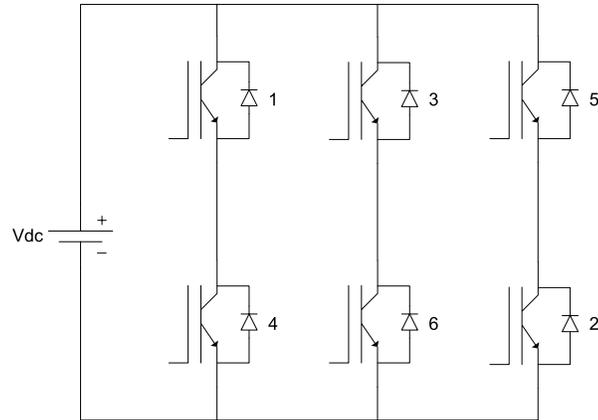
Figure 2.11 Inverter with IGBTs and Antiparallel Diodes

2.4.2 IGBTs

IGBTs provide high input impedance and are used for high voltage applications. The high input impedance allows the device to switch with a small amount of energy and for high voltage applications the device must have large blocking voltage ratings. The device behavior is described by parameters like voltage drop or on-resistance, turn on time and turn off time. Figure 2.12 shows the characteristic plot of the device (International rectifier IGBT (IRGIB10B60KD1) Appendix 1).
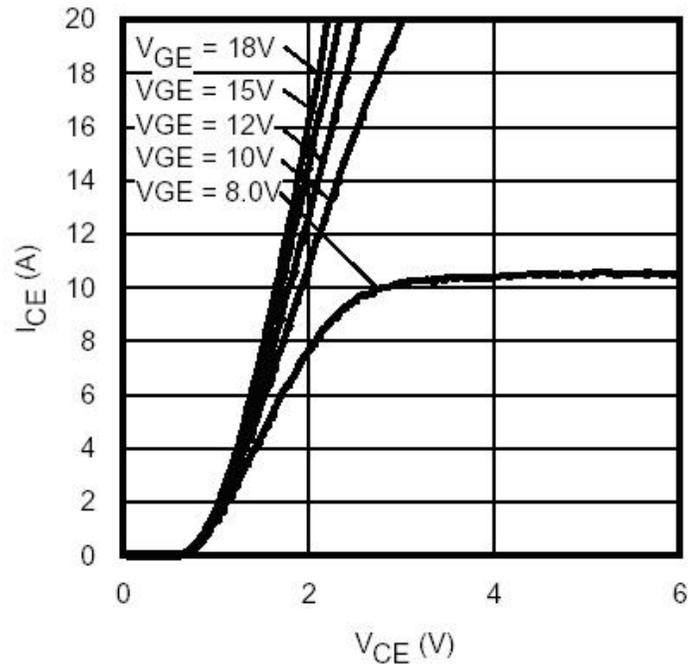
Figure 2.12 Typical IGBT Output Characteristics for IRGIB10B60KD1 (app. 1)

The symbolic representation and the equivalent circuit of an IGBT are shown in figure 2.13.
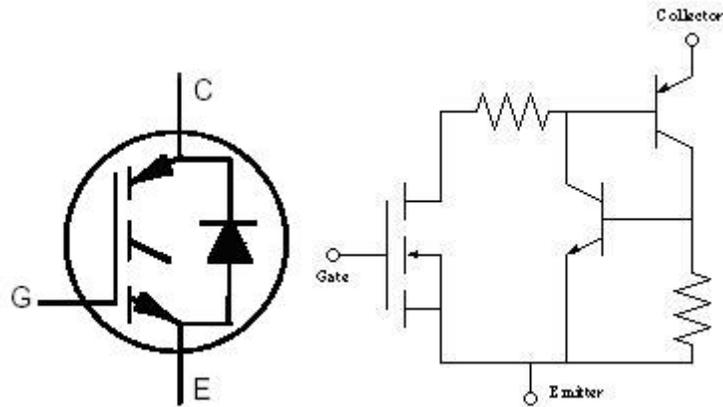
Figure 2.13 IGBT Symbol and Equivalent Circuit (app. 1)

2.4.3 Current Control

The power converter in a high-performance motor drive used in motion control essentially functions as a power amplifier, reproducing the low power level control signals generated in the field orientation controller at power levels appropriate for the driven machine. High-performance drives utilize control strategies which develop command signals for the AC machine currents. The basic reason for the selection of current as the controlled variable is the same as for the DC machine; the stator dynamics (effects of stator resistance, stator inductance, and induced EMF) are eliminated. Thus, to the extent that the current regulator functions as an ideal current supply, the order of the system under control is reduced and the complexity of the controller can be significantly simplified.

Current regulators for AC drives are complex because an AC current regulator must control both the amplitude and phase of the stator current. The AC drive current regulator forms the inner loop of the overall motion controller. As such, it must have the widest bandwidth in the system and must, by necessity, have zero or nearly zero steady-state error. Both current source inverters (CSI) and voltage source inverters (VSI) can be operated in controlled current modes. The current source inverter is a "natural" current supply and can readily be adapted to controlled current operation. The voltage source inverter requires more complexity in the current regulator but offers much higher bandwidth and elimination of current harmonics as compared to the CSI and is almost exclusively used for motion control applications.

Current controllers can be classified into two groups, hysteresis and PWM current controllers. Both types are discussed bellow.

2.4.3.1 *PWM Current Controller*

PWM current controllers are widely used. The switching frequency is usually kept constant. They are based in the principle of comparing a triangular carrier wave of desire switching frequency and is compared with error of the controlled signal. The error signal comes from the sum of the reference signal generated in the controller and the negative of the actual motor current. The comparison will result in a voltage control signal that goes to the gates of the voltage source inverter to generate the desire output. Its control will respond according to the error. If the error command is greater than the triangle waveform, the inverter leg is held switched to the positive polarity (upper switch on). When the error command is less than the triangle waveform, the inverter leg is switched to the negative polarity (lower switch on). This will generate a PWM signal like in figure 2.14. The inverter leg is forced to switch at the frequency of the triangle wave and produces an output voltage proportional to the current error command. The nature of the controlled output current consists of a reproduction of the reference current with high-frequency PWM ripple superimposed[23].
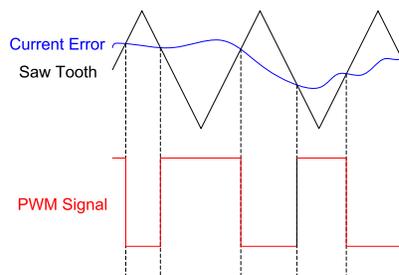

Figure 2.14 PWM current controller

29

2.4.3.2   Hysteresis current controller

Hysteresis current controller can also be implemented to control the inverter currents. The controller will generate the reference currents with the inverter within a range which is fixed by the width of the band gap. In this controller the desired current of a given phase is summed with the negative of the measured current. The error is fed to a comparator having a hysteresis band. When the error crosses the lower limit of the hysteresis band, the upper switch of the inverter leg is turned on. But when the current attempts to become less than the upper reference band, the bottom switch is turned on. Figure 2.15 shows the hysteresis band with the actual current and the resulting gate signals. This controller does not have a specific switching frequency and changes continuously but it is related with the band width [4] [23].
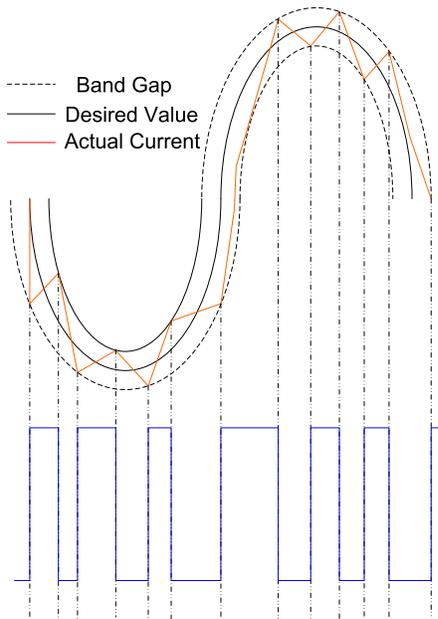
Figure 2.15 Hysteresis controller

3   MODELING OF PM DRIVE SYSTEM

This chapter deals with the detailed modeling of a permanent magnet synchronous motor. Field oriented control of the motor in constant torque and flux-weakening regions are discussed. Closed loop control of the motor is developed using a PI controller in the speed loop. Design of the speed controller is discussed.

3.1 Detailed Modeling of PMSM

Detailed modeling of PM motor drive system is required for proper simulation of the system. The d-q model has been developed on rotor reference frame as shown in figure 3.1. At any time t, the rotating rotor d-axis makes and angle θ_r with the fixed stator phase axis and rotating stator mmf makes an angle α with the rotor d-axis. Stator mmf rotates at the same speed as that of the rotor.
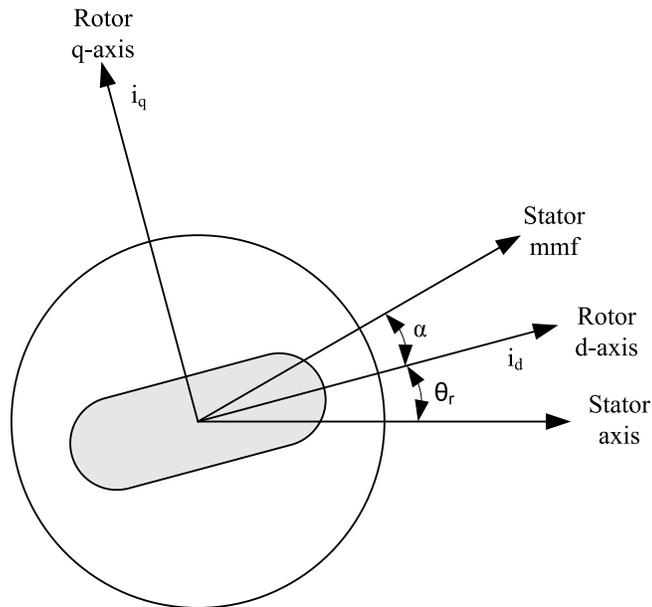
Figure 3.1 Motor Axis

31

The model of PMSM without damper winding has been developed on rotor reference frame using the following assumptions:

1) Saturation is neglected.

2) The induced EMF is sinusoidal.

3) Eddy currents and hysteresis losses are negligible.

4) There are no field current dynamics.

Voltage equations are given by:

$$V_q = R_s i_q + \omega_r \lambda_d + \rho \lambda_q \qquad \textbf{3.1}$$

$$V_d = R_s i_d - \omega_r \lambda_q + \rho \lambda_d \qquad \textbf{3.2}$$

Flux Linkages are given by

$$\lambda_q = L_q i_q \qquad \textbf{3.3}$$

$$\lambda_d = L_d i_d + \lambda_f \qquad \textbf{3.4}$$

Substituting equations 3.3 and 3.4 into 3.1 and 3.2

$$V_q = R_s i_q + \omega_r \left(L_d i_d + \lambda_f \right) + \rho L_q i_q \qquad \textbf{3.5}$$

$$V_d = R_s i_d - \omega_r L_q i_q + \rho \left(L_d i_d + \lambda_f \right) \qquad \textbf{3.6}$$

Arranging equations 3.5 and 3.6 in matrix form

$$\begin{pmatrix} V_q \\ V_d \end{pmatrix} = \begin{pmatrix} R_s + \rho L_q & \omega_r L_d \\ -\omega_r L_q & R_s + \rho L_d \end{pmatrix} \begin{pmatrix} i_q \\ i_d \end{pmatrix} + \begin{pmatrix} \omega_r \lambda_f \\ \rho \lambda_f \end{pmatrix} \qquad \textbf{3.7}$$

The developed torque motor is being given by

$$T_e = \frac{3}{2} \left(\frac{P}{2} \right) \left(\lambda_d i_q - \lambda_q i_d \right) \qquad \textbf{3.8}$$

The mechanical Torque equation is

$$T_e = T_L + B\omega_m + J\frac{d\omega_m}{dt}$$ **3.9**

Solving for the rotor mechanical speed form equation 3.9

$$\omega_m = \int\left(\frac{T_e - T_L - B\omega_m}{J}\right)dt$$ **3.10**

and

$$\omega_m = \omega_r\left(\frac{2}{P}\right)$$ **3.11**

In the above equations ω_r is the rotor electrical speed where as ω_m is the rotor mechanical speed.

3.1.1 Parks Transformation and Dynamic d q Modeling

The dynamic d q modeling is used for the study of motor during transient and steady state. It is done by converting the three phase voltages an currents to dqo variables by using Parks transformation[8].

Converting the phase voltages variables v_{abc} to v_{dqo} variables in rotor reference frame the following equations are obtained

$$\begin{bmatrix} V_q \\ V_d \\ V_o \end{bmatrix} = \frac{2}{3}\begin{bmatrix} \cos\theta_r & \cos(\theta_r - 120) & \cos(\theta_r + 120) \\ \sin\theta_r & \sin(\theta_r - 120) & \sin(\theta_r + 120) \\ 1/2 & 1/2 & 1/2 \end{bmatrix}\begin{bmatrix} V_a \\ V_b \\ V_c \end{bmatrix}$$ **3.12**

Convert V_{dqo} to V_{abc}

$$\begin{bmatrix} V_a \\ V_b \\ V_c \end{bmatrix} = \begin{bmatrix} \cos\theta_r & \sin\theta_r & 1 \\ \cos(\theta_r - 120) & \sin\theta_r - 120 & 1 \\ \cos(\theta_r + 120) & \sin(\theta_r + 120) & 1 \end{bmatrix}\begin{bmatrix} V_q \\ V_d \\ V_o \end{bmatrix}$$ **3.13**

33

3.1.2 Equivalent Circuit of Permanent Magnet Synchronous Motor

Equivalent circuits of the motors are used for study and simulation of motors. From the d-q modeling of the motor using the stator voltage equations the equivalent circuit of the motor can be derived. Assuming rotor d axis flux from the permanent magnets is represented by a constant current source as described in the following equation $\lambda_f = L_{dm} i_f$, figure 3.2 is obtained.
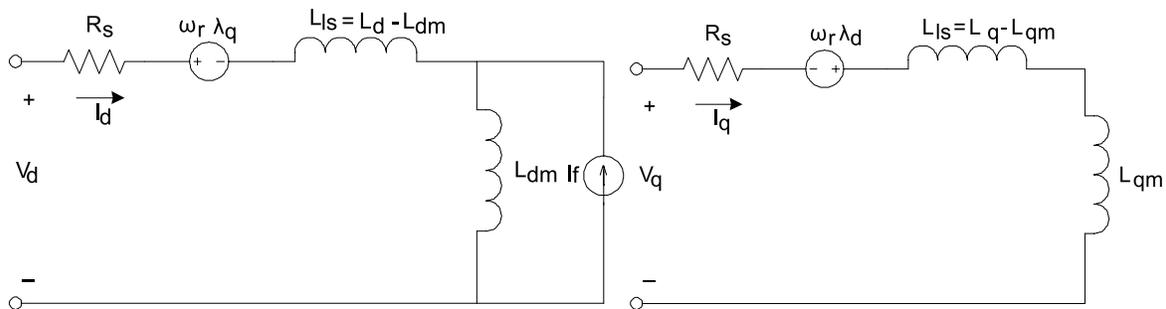

Figure 3.2 Permanent Magnet Motor Electric Circuit without Damper Windings

3.2 PM Motor Control

Control of PM motors is performed using field oriented control for the operation of synchronous motor as a dc motor. The stator windings of the motor are fed by an inverter that generates a variable frequency variable voltage. Instead of controlling the inverter frequency independently, the frequency and phase of the output wave are controlled using a position sensor as shown in figure 3.3.
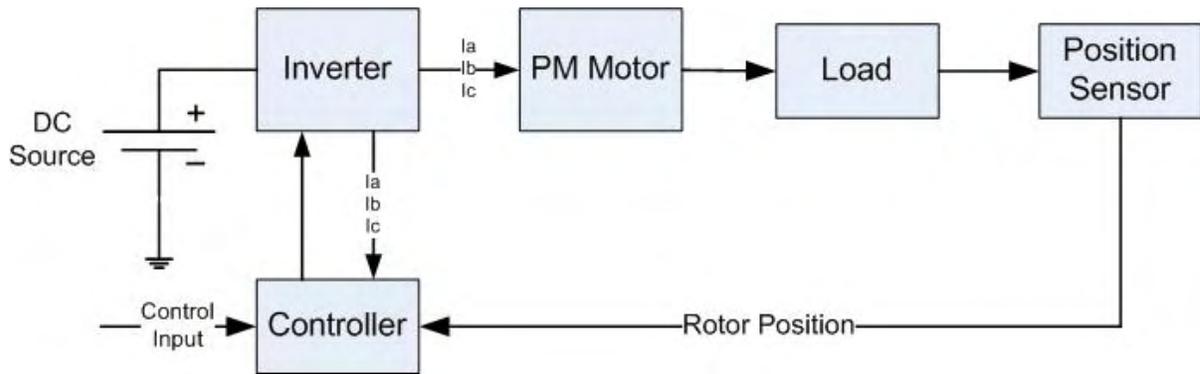
Figure 3.3 Self Control Synchronous Motor

Field oriented control was invented in the beginning of 1970s and it demonstrates that an induction motor or synchronous motor could be controlled like a separately excited dc motor by the orientation of the stator mmf or current vector in relation to the rotor flux to achieve a desired objective. In order for the motor to behave like DC motor, the control needs knowledge of the position of the instantaneous rotor flux or rotor position of permanent magnet motor. This needs a resolver or an absolute optical encoder. Knowing the position, the three phase currents can be calculated. Its calculation using the current matrix depends on the control desired. Some control options are constant torque and flux weakening. These options are based in the physical limitation of the motor and the inverter. The limit is established by the rated speed of the motor, at which speed the constant torque operation finishes and the flux weakening starts as shown in figure 3.4.

35
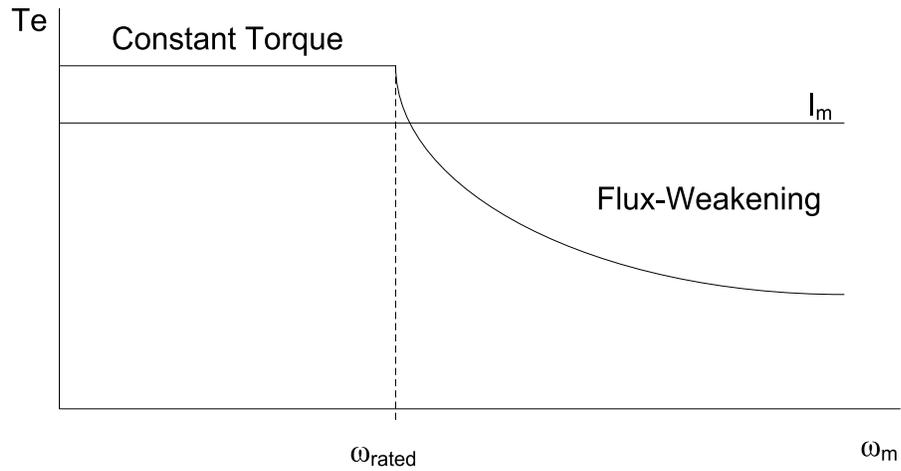
Figure 3.4 Steady State Torque versus Speed

3.2.1 Field Oriented Control of PM Motors

The PMSM control is equivalent to that of the dc motor by a decoupling control known as field oriented control or vector control. The vector control separates the torque component of current and flux channels in the motor through its stator excitation.

The vector control of the PM synchronous motor is derived from its dynamic model. Considering the currents as inputs, the three currents are:

$$i_a = I_m \sin(\omega_r t + \alpha) \qquad\qquad \textbf{3.14}$$

$$i_b = I_m \sin(\omega_r t + \alpha - \frac{2\pi}{3}) \qquad\qquad \textbf{3.15}$$

$$i_c = I_m \sin(\omega_r t + \alpha + \frac{2\pi}{3}) \qquad\qquad \textbf{3.16}$$

Writing equations 3.14 to 3.16 in the matrix form:

36

$$\begin{pmatrix} i_a \\ i_b \\ i_c \end{pmatrix} = \begin{pmatrix} \cos(\omega_r t + \alpha) \\ \cos(\omega_r t + \alpha - \dfrac{2\pi}{3}) \\ \cos(\omega_r t + \alpha + \dfrac{2\pi}{3}) \end{pmatrix} (I_m) \qquad \textbf{3.17}$$

Where α is the angle between the rotor field and stator current phasor, ω_r is the electrical rotor speed.

The previous currents obtained are the stator currents that must be transformed to the rotor reference frame with the rotor speed ω_r, using Park's transformation. The q and d axis currents are constants in the rotor reference frames since α is a constant for a given load torque. As these constants, they are similar to the armature and field currents in the separately excited dc machine. The q axis current is distinctly equivalent to the armature current of the dc machine; the d axis current is field current, but not in its entirety. It is only a partial field current; the other part is contributed by the equivalent current source representing the permanent magnet field. For this reason the q axis current is called the torque producing component of the stator current and the d axis current is called the flux producing component of the stator current.

Substituting equation 3.17 and 3.12 is obtain i_d and i_q in terms of I_m as follows

$$\begin{pmatrix} i_q \\ i_d \end{pmatrix} = I_m \begin{pmatrix} \sin\alpha \\ \cos\alpha \end{pmatrix} \qquad \textbf{3.18}$$

Using equations 3.1, 3.2, 3.8 and 3.18 the electromagnetic torque equation is obtained as given below.

$$T_e = \frac{3}{2} \cdot \frac{P}{2} \left[\frac{1}{2}(L_d - L_q)I_m^2 \sin 2\alpha + \lambda_f I_m \sin \alpha \right]$$　　　　**3.19**

3.2.1.1 *Constant torque operation*

Constant torque control strategy is derived from field oriented control, where the maximum possible torque is desired at all times like the dc motor. This is performed by making the torque producing current i_q equal to the supply current I_m. That results in selecting the α angle to be 90 ° degrees according to equation 3.18. By making the i_d current equal to zero the torque equation can be rewritten as:

$$T_e = \left(\frac{3}{2}\right)\left(\frac{P}{2}\right)\lambda_f \cdot i_q$$　　　　**3.20**

Assuming that:

$$k_t = \left(\frac{3}{2}\right)\left(\frac{P}{2}\right)\lambda_f$$　　　　**3.21**

The torque is give by

$$T_e = k_t \cdot i_q$$　　　　**3.22**

Like the dc motor, the torque is dependent of the motor current.

3.2.1.2 *Flux-weakening*

Flux weakening is the process of reducing the flux in the d axis direction of the motor which results in an increased speed range.

The motor drive is operated with rated flux linkages up to a speed where the ratio between the induced emf and stator frequency (V/f) is maintained constant. After the base frequency, the V/f ratio is reduced due to the limit of the inverter dc voltage source which is fixed. The weakening of the field flux is required for operation above the base frequency.

This reduces the V/f ratio. This operation results in a reduction of the torque proportional to a change in the frequency and the motor operates in the constant power region[22].

The rotor flux of PMSM is generated by permanent magnet which can not be directly reduced as induction motor. The principle of flux-weakening control of PMSM is to increase negative direct axis current and use armature reaction to reduce air gap flux, which equivalently reduces flux and achieves the purpose of flux-weakening control[28].

This method changes torque by altering the angle between the stator MMF and the rotor d axis. In the flux weakening region where $\omega_r > \omega_{rated}$ angle α is controlled by proper control of i_d and i_q for the same value of stator current. Since i_q is reduced the output torque is also reduced. The angle α can be obtained as:

$$\alpha = Tan^{-1}\left(\frac{i_q}{i_d}\right)$$ 3.23

The current I_m is related to i_d and i_q by:

$$I_m = \sqrt{i_d^2 + i_q^2}$$ 3.24

Flux-weakening control realization

The realization process of equivalent flux-weakening control is as follows,

1) Measuring rotor position and speed ω_r from a sensor which is set in motor rotation axis.

2) The motor at the flux weakening region with a speed loop, Te* is obtained from the PI controller.

4) Calculate I_q* using equation 3.20 ($i_q = \dfrac{T_e^*}{\left(\dfrac{3}{2}\right)\left(\dfrac{P}{2}\right)\lambda_f}$)

39

5) Calculate I$_d$* using equation:
$$i_d^* = \frac{\lambda_d - \lambda_f}{L_d}$$

6) Calculate α using equation 3.23.

7) Using α and rotor position the controller will generate the reference currents as per equation 3.17.

8) Then the current controller makes uses of the reference signals to control the inverter for the desired output currents.

9) The load torque is adjust to the maximum available torque for the reference speed
$$T_L = T_{e(rated)} \frac{\omega_{rated}}{\omega_r}.$$

3.3 Speed Control of PM Motor

Many applications, such as robotics and factory automation, require precise control of speed and position. Speed Control Systems allow one to easily set and adjust the speed of a motor. The control system consists of a speed feedback system, a motor, an inverter, a controller and a speed setting device. A properly designed feedback controller makes the system insensible to disturbance and changes of the parameters.

The purpose of a motor speed controller is to take a signal representing the demanded speed, and to drive a motor at that speed. Closed Loop speed control systems have fast response, but become expensive due to the need of feed back components such as speed sensors.

3.3.1 *Implementation* of the Speed Control Loop

For a PM motor drive system with a full speed range the system will consist of a motor, an inverter, a controller (constant torque and flux weakening operation, generation of reference currents and PI controller) as shown in figure 3.5.
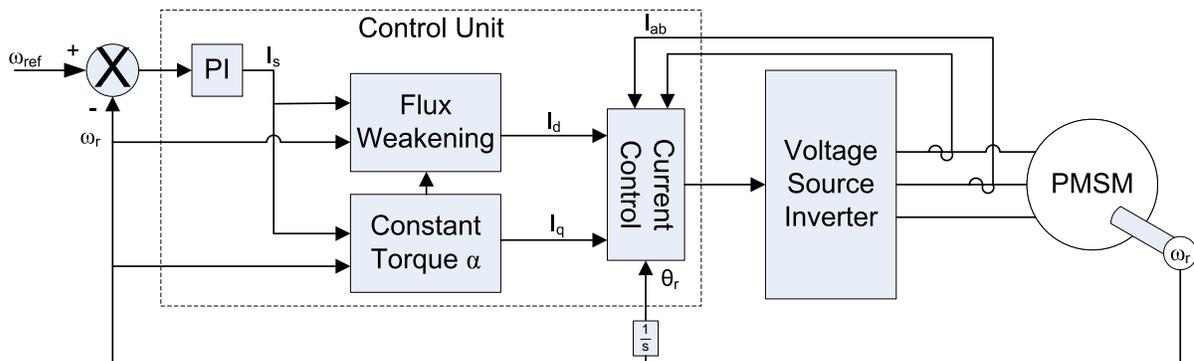
Figure 3.5 Block Diagram

The operation of the controller must be according to the speed range. For operation up to rated speed it will operate in constant torque region and for speeds above rated speed it will operate in flux-weakening region. In this region the d-axis flux and the developed torque are reduced. The process can be easily understood with the flow diagram in figure 3.6.

41
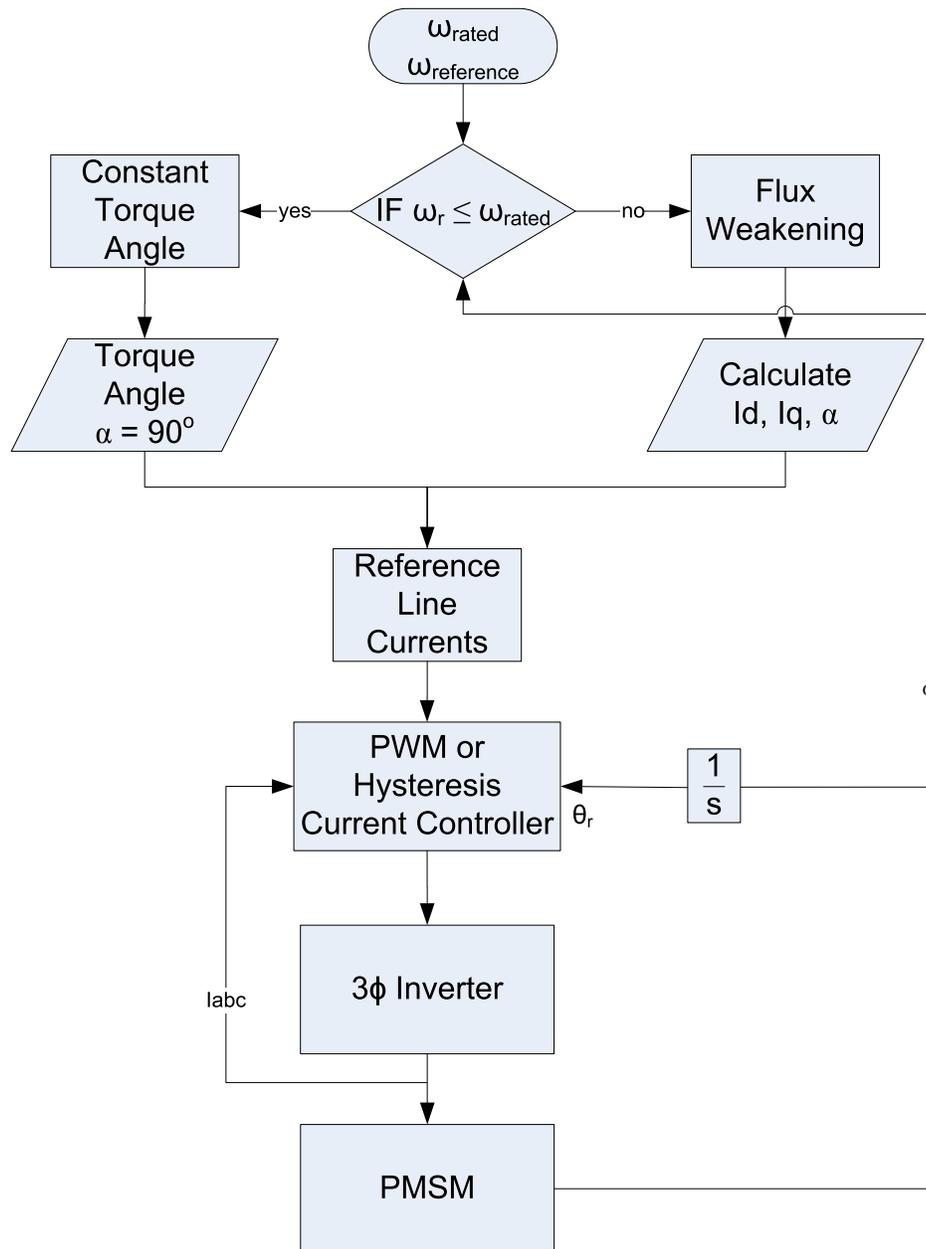
Figure 3.6 System Flow Diagram

Speed controller calculates the difference between the reference speed and the actual

speed producing an error, which is fed to the PI controller. PI controllers are used widely for

motion control systems. They consist of a proportional gain that produces an output

proportional to the input error and an integration to make the steady state error zero for a step

change in the input. Block diagram of the PI controller is shown in figure 3.7.
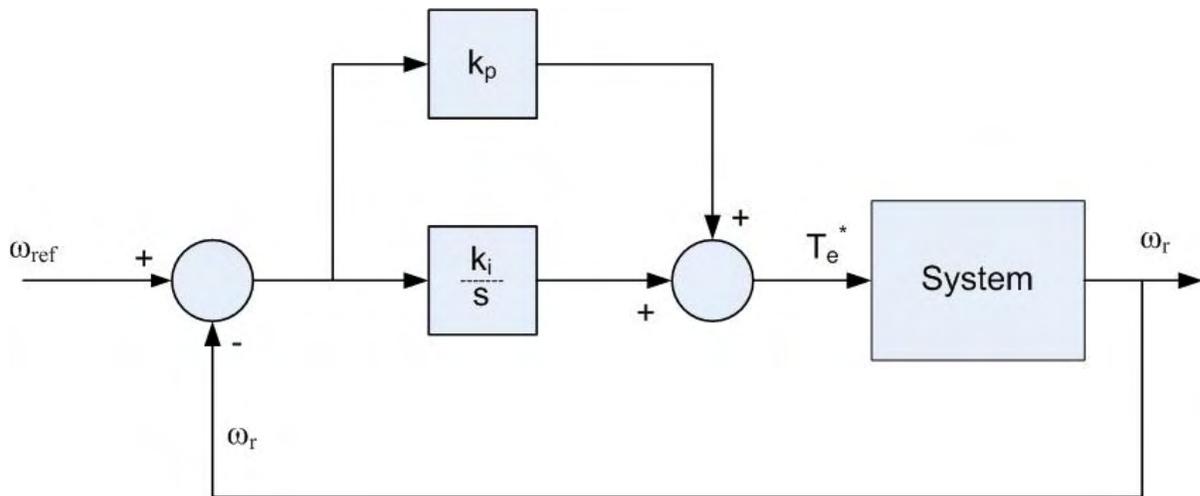
Figure 3.7 PI Controller

Speed control of motors mainly consist of two loops the inner loop for current and the

outer loop for speed. The order of the loops is due to their response, how fast they can be

changed. This requires a current loop at least 10 times faster than the speed loop.

Since the PMSM is operated using field oriented control, it can be modeled like a dc

motor. The design begins with the innermost current loop by drawing the block diagram. But

in PMSM drive system the motor has current controllers which make the current loop. The

current control is performed by the comparison of the reference currents with the actual

motor currents.

The design of the speed loop assumes that the current loop is at least 10 times faster than speed loop, allowing to reduce the system block diagram by considering the current loop to be of unity gain as shown in figure 3.8.
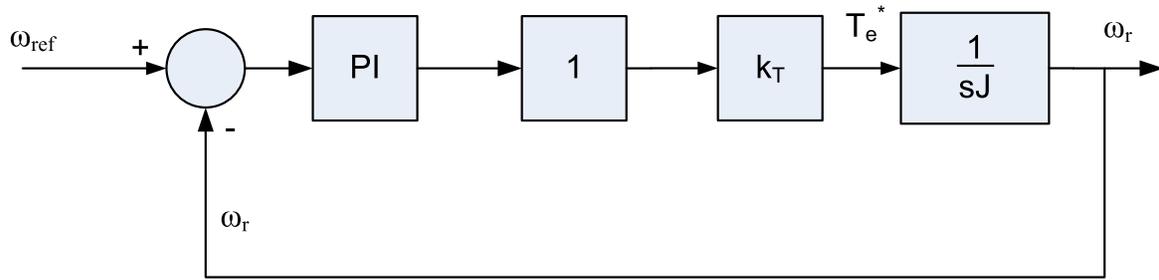
Figure 3.8 Block Diagram of Speed Loop

The open loop transfer function of the motor is given by:

$$GH_{(s)} = \left(\frac{k_i k_T \alpha}{J}\right)\left(\frac{1 + s\,{k_p}/{k_i}}{s^2}\right)$$ **3.25**

$k_T = $ PM flux $= \lambda_f$

The crossover frequency has been selected an order smaller than the current loop. To satisfy dynamic response without oscillations the phase margin (ϕ_{PM}) should be greater than 45°, preferably close to 60°. Knowing the motor parameters and phase margin, the k_i and k_p gains can be obtained for the motor controller using equations 3.26 and 3.27.

Phase Margin $= \phi_{OL} + 180°$

$$\left|\frac{k_i k_T \alpha}{J \cdot s^2}\left(1 + s\,{k_p}/{k_i}\right)\right|_{s=j\omega} = 1$$ **3.26**

$$\text{Angle} \left| \frac{k_i k_T \alpha}{J \cdot s^2} \left(1 + s \frac{k_p}{k_i} \right) \right| = 180° + \phi_{PM} \qquad \qquad \textbf{3.27}$$

The gains for the speed controller was obtained using the motor parameters and by selecting a crossover frequency. The selected values are:

f_c (crossover frequency)= 100Hz $J = 0.000179$ $k_T = \lambda_f = 0.272$

Using equation 3.26 and 3.27 and motor parameters the values of ki and kp are obtained as 129.9014 and 0.3581 respectively.

4 DRIVE SYSTEM SIMULATION IN SIMULINK

This chapter describes different tools available for electrical and electronic systems simulation and then justification is given for selecting Simulink for the PMSM system. Block by block an explanation is given for Simulink simulation of the drive system.

4.1 Simulation Tools

Study of electric motor drives needs the proper selection of a simulation tool. Their complex models need computing tools capable of performing dynamic simulations. Today with the growth in computational power there is a wide selection of software titles available for electrical simulations such as ACSL, ESL, EASY5, and PSCSP are for general systems and SPICE2, EMTP, and ATOSEC5 for simulating electrical and electronic circuits. IESE and SABER are examples of general-purpose electrical network simulation programs that have provisions for handling user-defined modules. SIMULINK® is a toolbox extension of the MATLAB program. It is a program for simulating dynamic systems [13].

Simulink has the advantages of being capable of complex dynamic system simulations, graphical environment with visual real time programming and broad selection of tool boxes[12]. The simulation environment of Simulink has a high flexibility and expandability which allows the possibility of development of a set of functions for a detailed analysis of the electrical drive [12]. Its graphical interface allows selection of functional blocks, their placement on a worksheet, selection of their functional parameters interactively, and description of signal flow by connecting their data lines using a mouse device. System

blocks are constructed of lower level blocks grouped into a single maskable block. Simulink simulates analogue systems and discrete digital systems[16].

4.2 Simulink Simulation of PMSM Drive

The PM motor drive simulation was built in several steps like abc phase transformation to dqo variables, calculation torque and speed, and control circuit.

The abc phase transformation to dqo variables is built using Parks transformation and for the dqo to abc the reverse transformation is used. For simulation purpose the voltages are the inputs and the current are output. Parks transformation used for converting Vabc to Vdqo is shown in figure 4.1 and the reverse transformation for converting Idqo to Iabc is shown in figure 4.2.
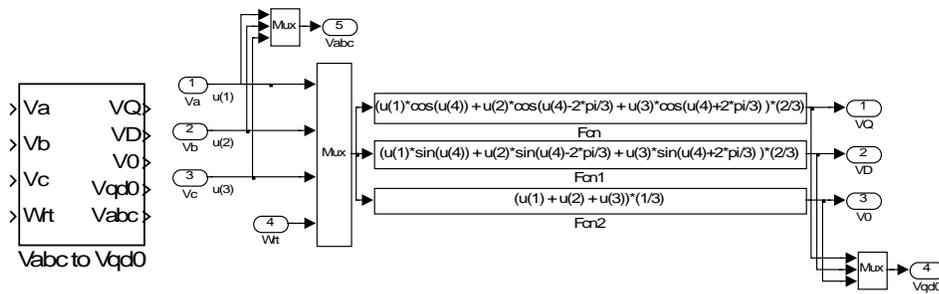
Figure 4.1 Vabc to Vdqo block
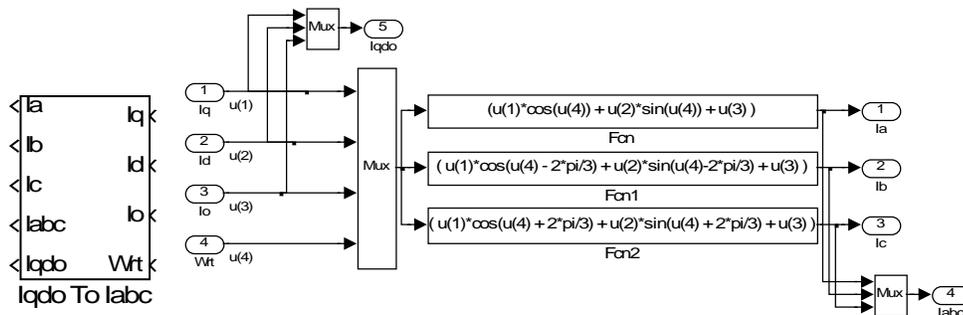
Figure 4.2 Idqo to Iabc block

The d and q axis motor circuits built using Simulink elements are shown in figure 4.3
and 4.4.

Figure 4.3 d-axix circuit
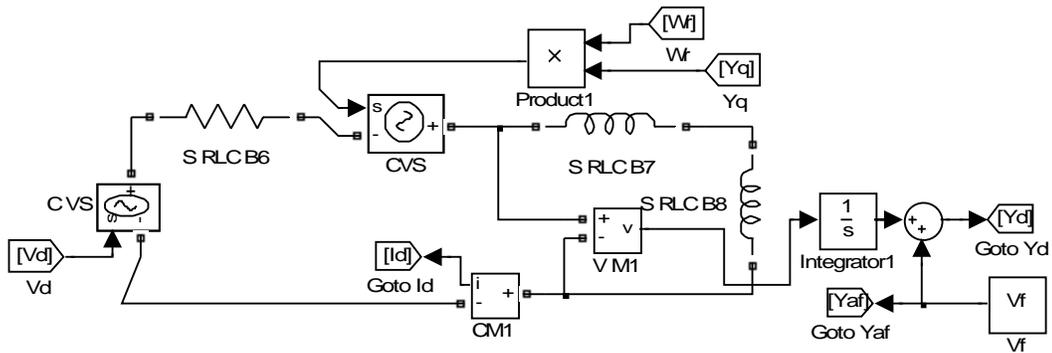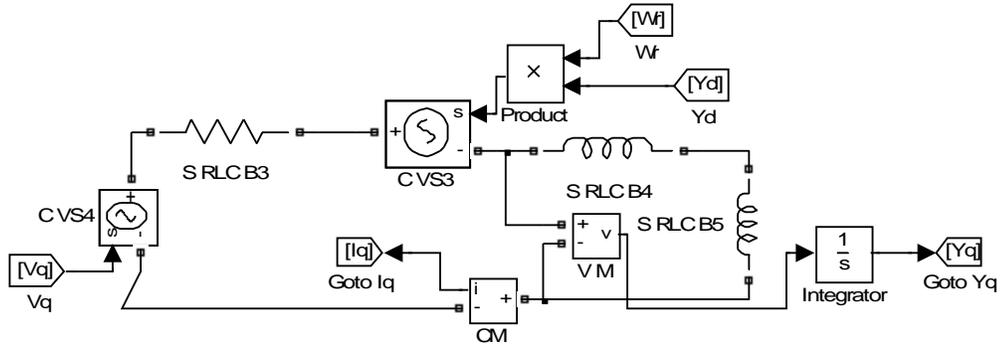
Figure 4.4 q-axis circuit

Figure 4.5 shows the torque block in Simulink. This block is developed using
equation 3.8 for torque developed.
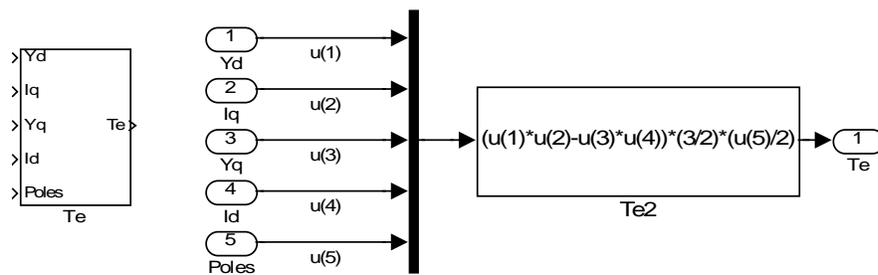
Figure 4.5 Torque Block

48

The speed of the motor is obtain using figure 4.5 and equation 3.9. The developed speed block is shown in figure 4.6.
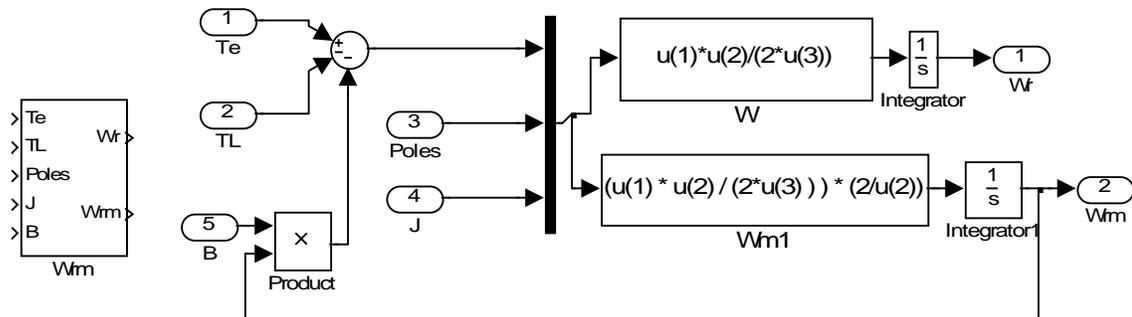
Figure 4.6 Speed Block

The vector control requires a block for the calculation of the reference current using the α angle, the position of the rotor and the magnitude of the Im. The block is shown in figure 4.7. It is built using equation 3.17.
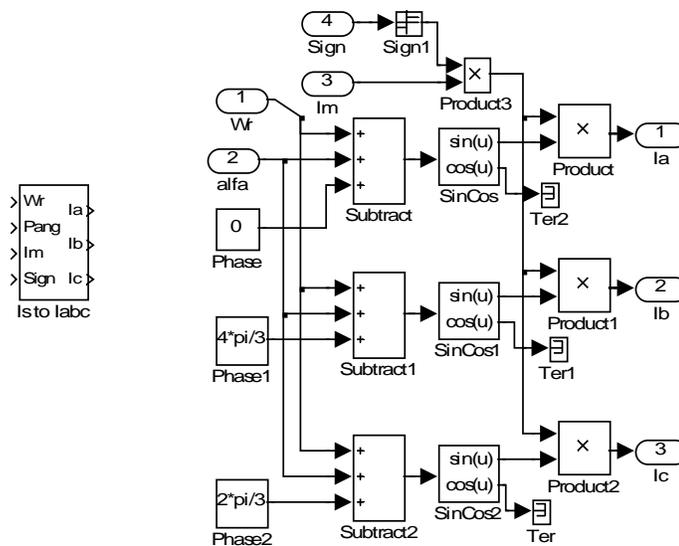
Figure 4.7 Vector Control Reference Current Block

The inverter is implemented in Simulink as shown in figure 4.8. The inverter consists of the "universal bridge" block from the power systems tool box with the parameters of the IGBT that was presented in chapter 2. The voltages and currents in the motor and in all the devices of the inverter can be obtained. The losses in the inverter and motor can be calculated.
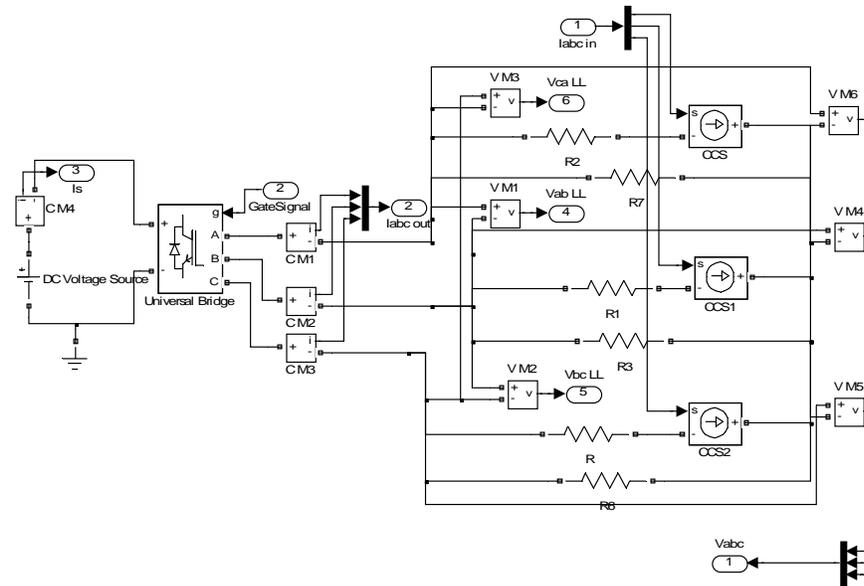
Figure 4.8 Voltage Source Inverter

For proper control of the inverter using the reference currents, current controllers are implemented to generate the gate pulses for the IGBT's. Current controllers used are shown in figure 4.9 and 4.10.
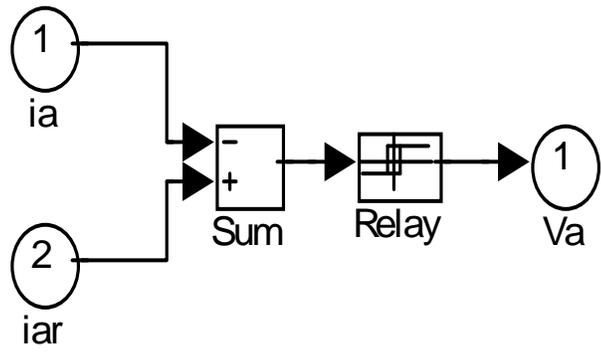
Figure 4.9 Hysteresis Current Controller
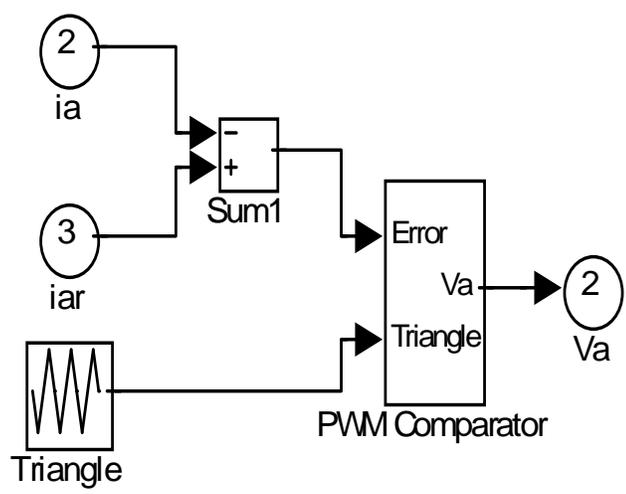
Figure 4.10 PWM Current Controller

Using all the drive system blocks the complete system block has been developed as shorn in figure 4.11.

Figure 4.11 PM Motor Drive System in Simulink

5 SIMULATION RESULTS

This chapter deals with the simulation results of PMSM drive system. The parameters of the motor and IGBT parameters are also given. Comparative study of the current controllers used in the system is given in tabular form.

5.1 Simulation Results

The system built in Simulink for a PMSM drive system has been tested with the two current control methods, Hysteresis and PWM, at the constant torque and flux-weakening regions of operation. The motor parameters used for simulation are given in table 5.1. These parameters were taken from reference [7]. IGBT parameters of the inverter are given in Appendix1.

The motor is operated with constant torque up to its rated speed and beyond that rated speed flux-weakening mode is adopted. Simulation results are given at electrical speeds of 200 radians per second (31 Hz) and 600 radians per second (95 Hz). The above speeds represent below and above rated speed of the motor.

Table 5.1   Interior Permanent Magnet Motor Parameters

Symbol	Name	Value
V_{LL}	Rated Voltage	220 V
Pout	magnetic flux	900w
P	Number of Poles	4
ω_m	Rated Speed	1700 rpm
Rs	Stator Resistance	4.3 Ω
λ_{af}	PM Flux Linkage	0.272 Wbturns
Ld	q-axis Inductance	27 mH
Ld	d-axis Inductance	67 mH
Is	Rated Current	3 A
Ismax	Maximung Current	2Israted
J	Motor Inertia	0.000179 kg m^2

The simulation was carried out using two current control techniques to study the performance of the motor drive. The techniques are Hysteresis current control and PWM current control. The plots of current, torque and speed are given for both cases.

5.1.1 Simulation for Operation at 200 rad/s

Hysteresis Current Control
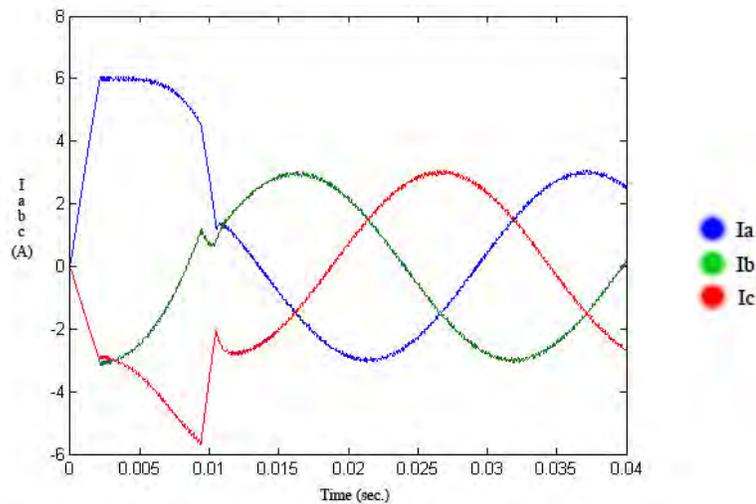
Figure 5.1 Iabc Currents with Hysteresis Control at 200 rad/s

Figure 5.1 shows the three phase currents drawn by the motor as a result of the hysteresis current control. The currents are obtained using Park's reverse transformation. It is clear that the current is non sinusoidal at the starting and becomes sinusoidal when the motor reaches the controller command speed at steady state. The corresponding dq component of current is given in figure 5.2. Since field oriented control is used the value of id is zero.
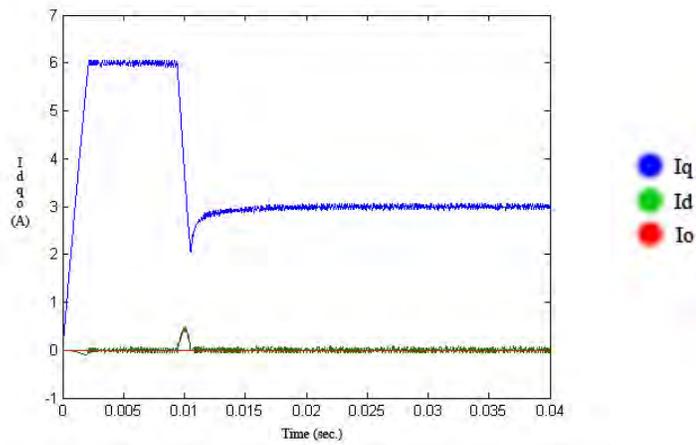
Figure 5.2 Idqo Currents with Hysteresis Control at 200 rad/s

Figure 5.3 shows the developed torque of the motor. The starting torque is twice the steady state value. The steady torque is 2.5 Nm.
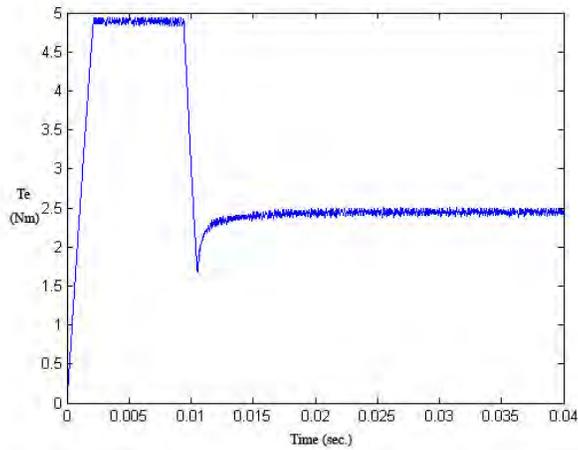
Figure 5.3 Developed Torque with Hysteresis Control at 200 rad/s
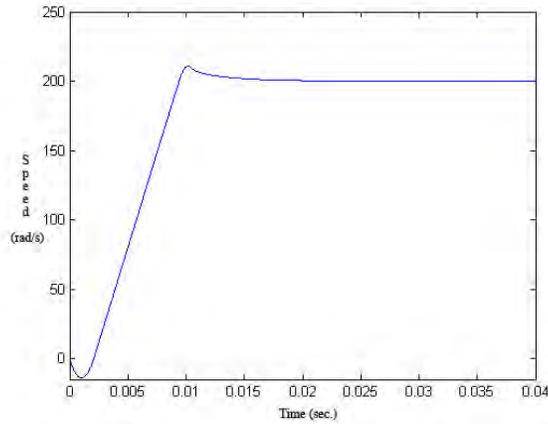
Figure 5.4 Motor Electrical Speed with Hysteresis Control at 200 rad/s

Figure 5.4 shows a variation of the speed with time. The steady state speed is the same as that of the commanded reference speed.
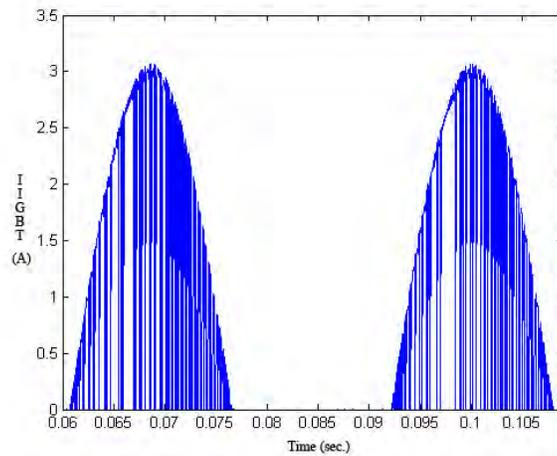

Figure 5.5 IGBT Current with Hysteresis Control at 200 rad/s

Figure 5.5 presents the waveform of the current flowing through the IGBT. The current pulses appear to be similar but since the switching frequency is dependent on the error in the hysteresis control the pulses widths differ. The average switching freqency is about 5 kHz.
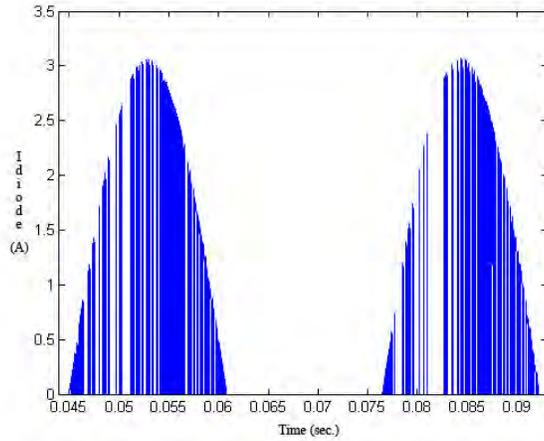
Figure 5.6 Diode Current with Hysteresis Control at 200 rad/s

Figure 5.6 shows the waveform of the current flowing through an antiparallel diode.
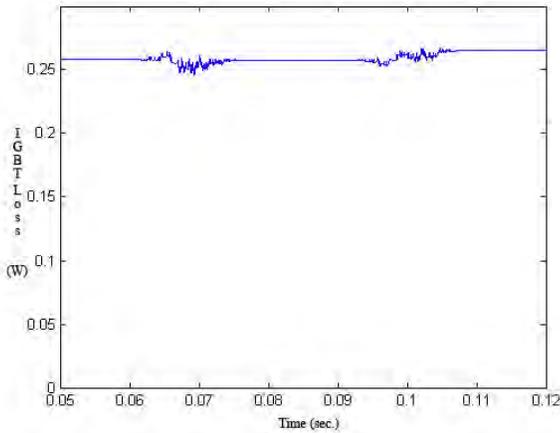
Figure 5.7 IGBT Average Power Loss with Hysteresis Control at 200 rad/s

Figure 5.7 shows the conduction loss in each IGBT at steady state. The voltage across the device is multiplied by the current through the device at every instant and the average of the instantaneous power is plotted.
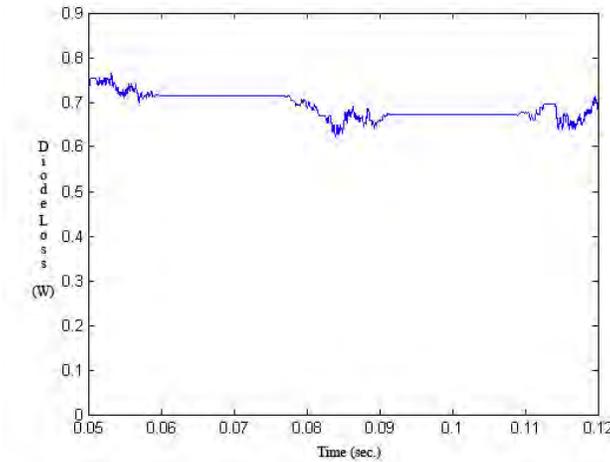
Figure 5.8 Diode Loss for Hysteresis Control at 200 rad/s

Figure 5.8 shows the average power loss in the diode. This is obtained from the instantaneous power calculated by multiplying voltage across the diode and current through it.
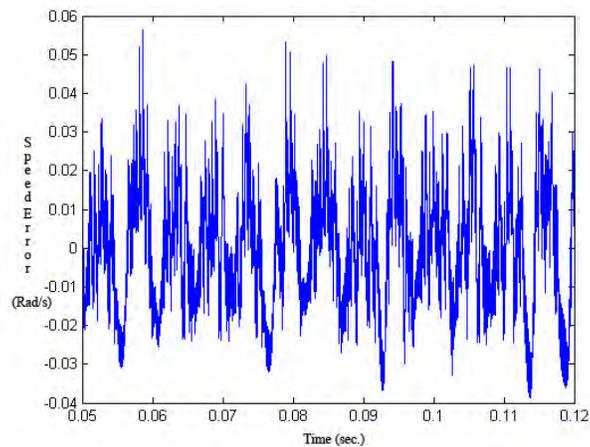
Figure 5.9 Speed Error for Hysteresis Control at 200 rad/s

Figure 5.9 shows the speed error plot for hysteresis control. The drive speed loop operates to maintain the command speed within an error represented in the speed error plot.

58

The above plots have been repeated with PWM control for comparing hysteresis control with PWM control.

PWM Current Control
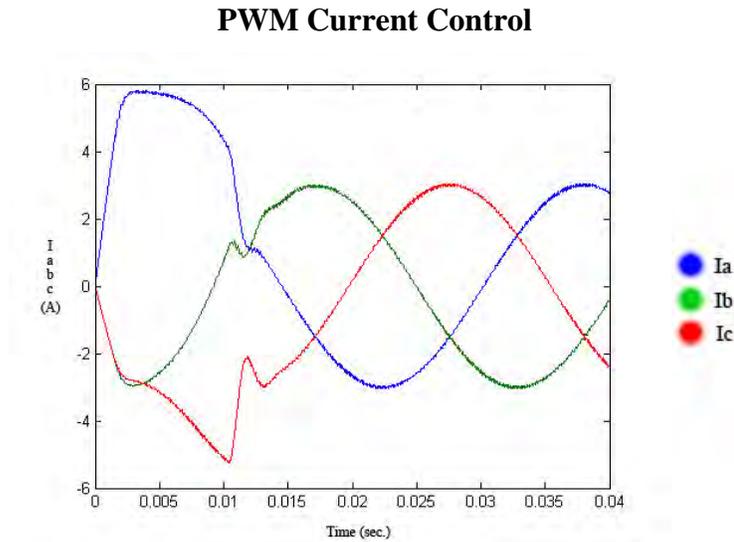
Figure 5.10 Iabc Currents with PWM Control at 200 rad/s

Figure 5.10 shows the three phase currents as a result of the PWM current control obtained from Park's reverse transformation. It is clear that the current is non sinusoidal at the starting and becomes sinusoidal when the motor reaches the controller command speed at steady state. The corresponding dq component of current is given in figure 5.11 with id almost equal to zero for constant torque operation.
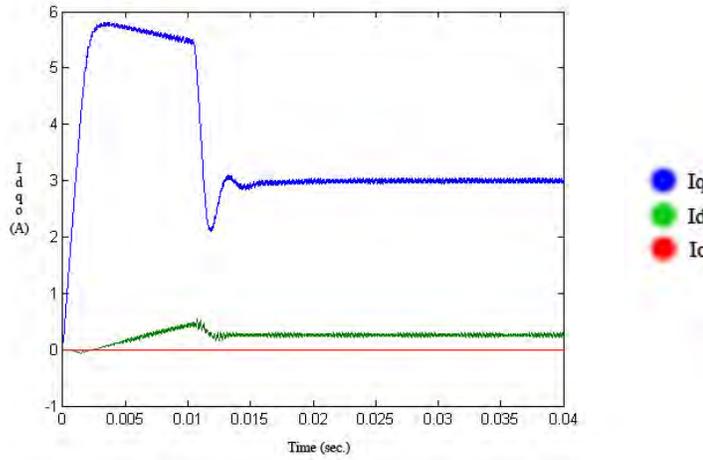
Figure 5.11 Idqo Currents with PWM Control at 200 rad/s
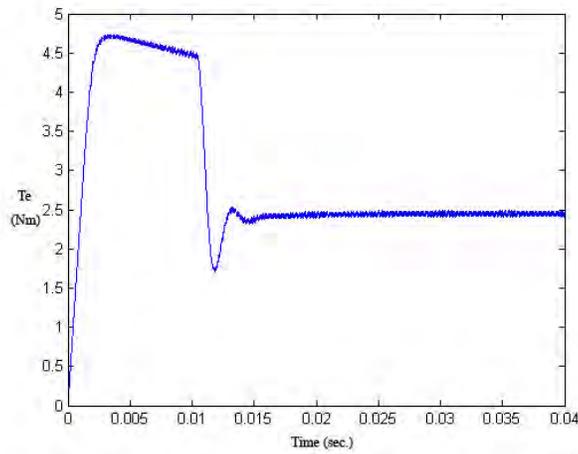
Figure 5.12 Developed Torque with PWM Control at 200 rad/s

Figure 5.12 shows the developed torque of the motor. The starting torque is twice the steady state value. The developed torque is the same as the load torque (2.5Nm) under steady state condition.
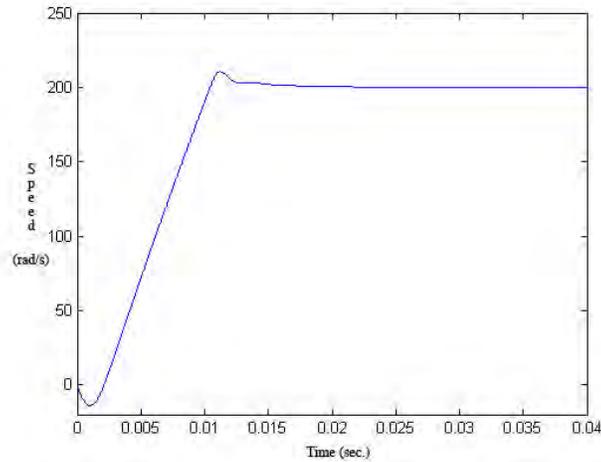
Figure 5.13 Motor Electrical Speed with PWM Controller at 200 rad/s

Figure 5.13 shows a variation of the speed with time. The steady state speed is the same as that of the commanded reference speed.
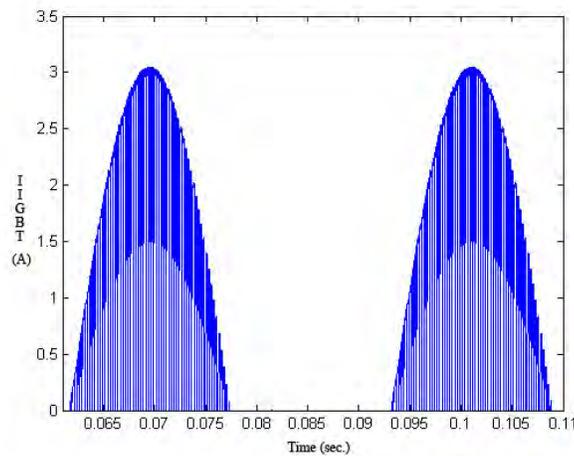

Figure 5.14 IGBT Current with PWM Controller at 200 rad/s

Figure 5.14 presents the waveform of the current flowing through the IGBT. The current pulses are similar. In this case the switching frequency is constant.

61
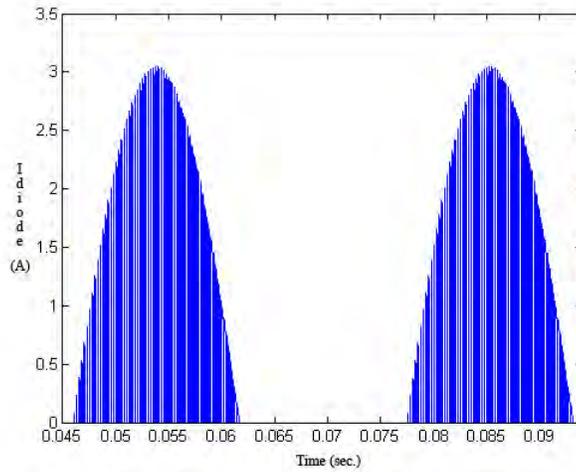
Figure 5.15 Diode Current with PWM Control at 200 rad/s

Figure 5.15 shows the waveform of the current flowing through the antiparallel diode.
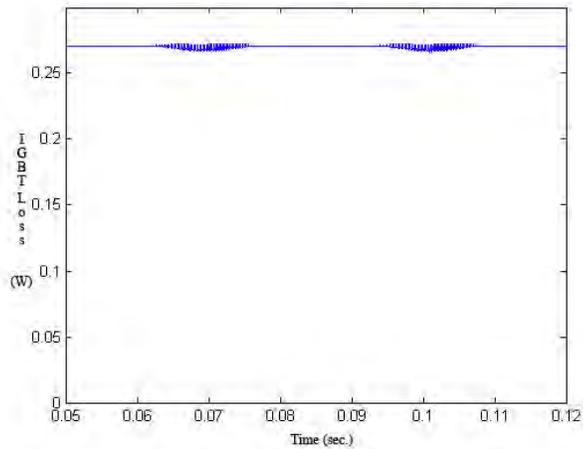
Figure 5.16 IGBT Average Power Loss with PWM Control at 200 rad/s

Figure 5.16 shows the average conduction loss in each IGBT at steady state. The voltage across the device is multiplied by the current through the device at each instant and the average is taken.
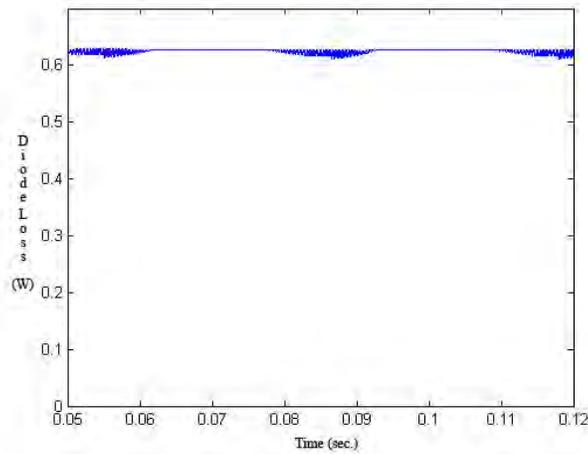
Figure 5.17 Diode Average Power Loss with PWM Control at 200 rad/s

Figure 5.17 shows the average power loss in the diode.
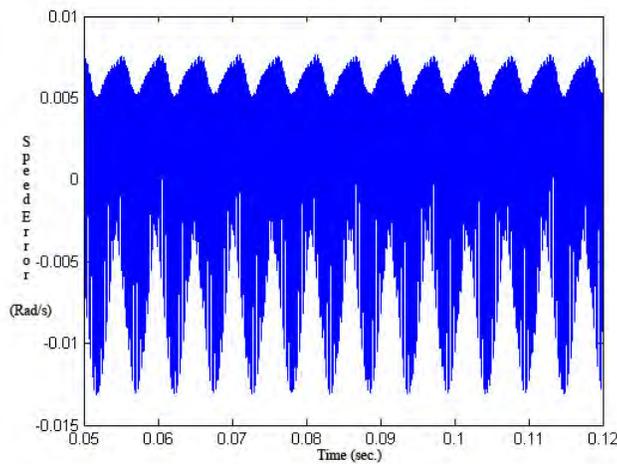
**Figure 5.18 Speed Error with PWM Control at 200 rad/s**

Figure 5.18 shows the speed error plot for PWM control. The drive speed loop operates to maintain the command speed within an error represented in the speed error plot. The speed error is practically zero with PWM control.

5.1.2 Simulation for Operation at Higher Speed of 600 rad/s

Hysteresis Current Control
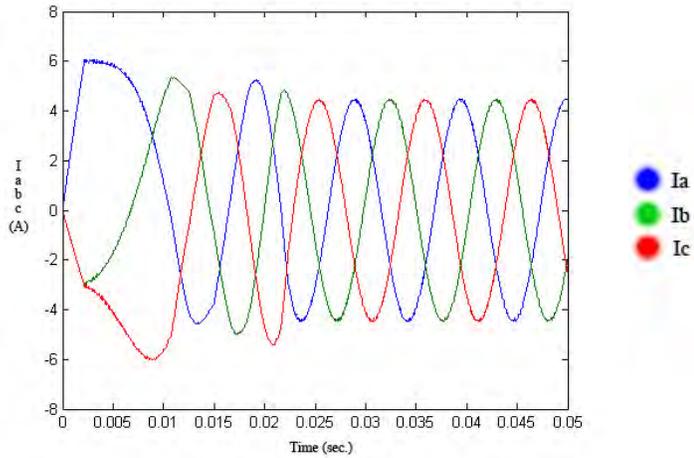
Figure 5.19 Iabc Currents with Hysteresis Control at 600 rad/s

Figure 5.19 shows the three phase currents as a result of the hysteresis current control obtained from Park's reverse transformation. It is clear that the current is non sinusoidal at the starting and becomes sinusoidal when the motor reaches the controller command speed of 600 rad/sec at steady state. The corresponding dq component of current is given in figure 5.20. Both d and q axis current are present. However the q axis current is very small since the torque gets very much reduced at higher speed, operating at constant power region.
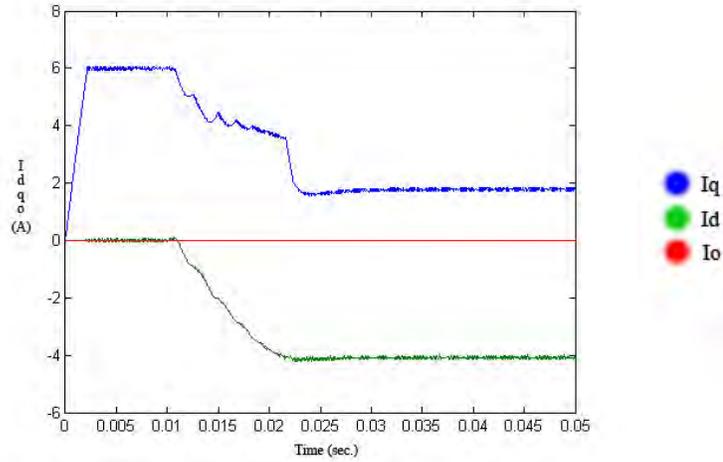
Figure 5.20 Idqo Currents with Hysteresis Control at 600 rad/s
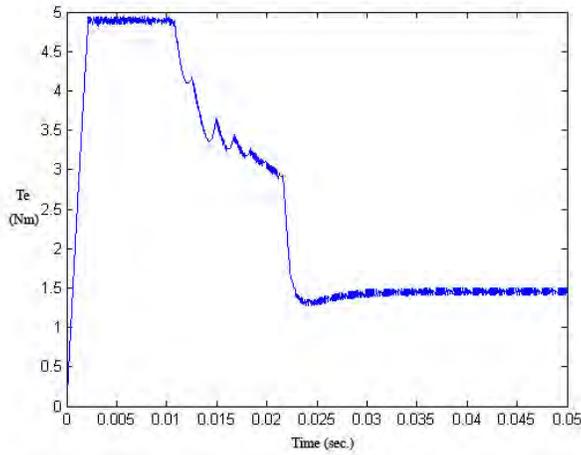
Figure 5.21 Developed Torque with Hysteresis Control at 600 rad/s

Figure 5.21 shows the developed torque of the motor. The starting torque is quiet high and the steady state value of torque is reduced to 1.5 Nm at this speed. At this speed the motor is operating in the constant power region.
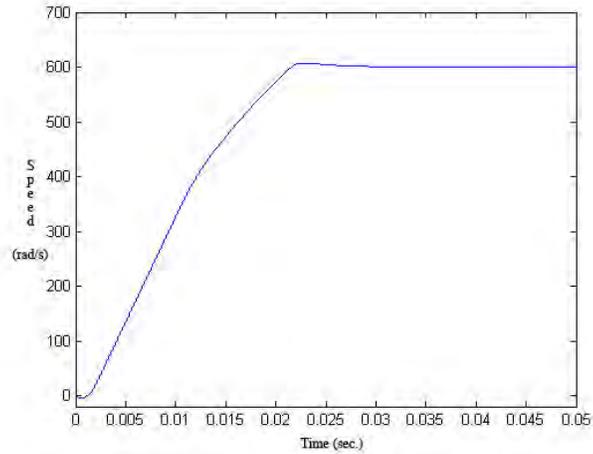
Figure 5.22 Motor Electrical Speed with Hysteresis Control at 600 rad/s

Figure 5.22 shows a variation of the speed with time. The steady state speed is the same as that of the commanded reference speed of 600 rad/sec.
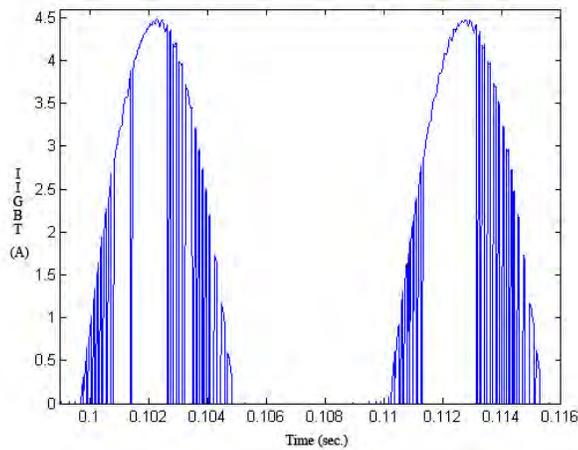
Figure 5.23 IGBT Current with Hysteresis Control at 600 rad/s

Figure 5.23 presents the waveform of the current flowing through the IGBT. The current pulses appear to be similar but since the switching frequency is dependent on the hysteresis band width, the pulses widths differ.

66
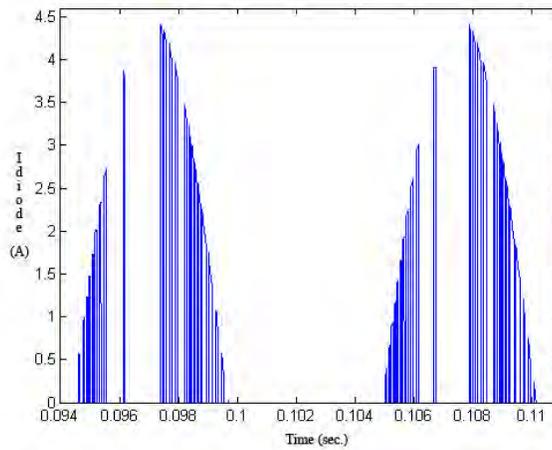
**Figure 5.24 Diode Current with Hysteresis Control at 600 rad/s**

Figure 5.24 shows the waveform of the current flowing through the antiparallel diode.
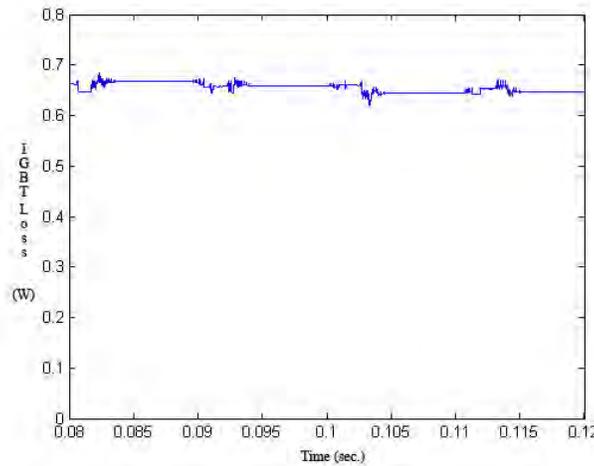
Figure 5.25 IGBT Average Power Loss with Hysteresis Control at 600 rad/s

Figure 5.25 shows the average conduction loss in each IGBT at steady state. The voltage across the device is multiplied by the current through the device and the average is taken.

67
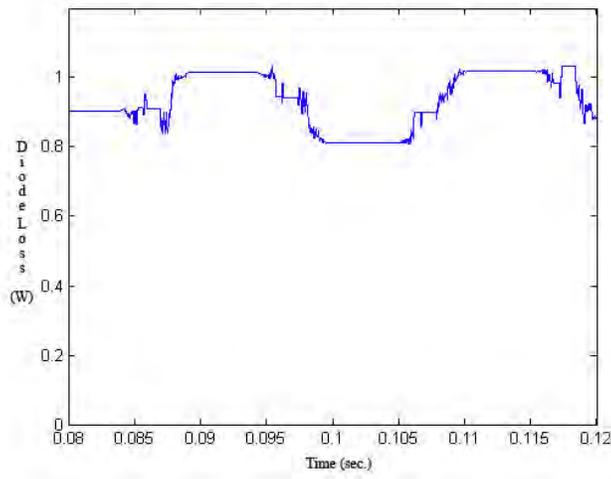
**Figure 5.26 Diode Average Power Loss with Hysteresis Control at 600 rad/s**

Figure 5.26 shows the average power loss in the diode.
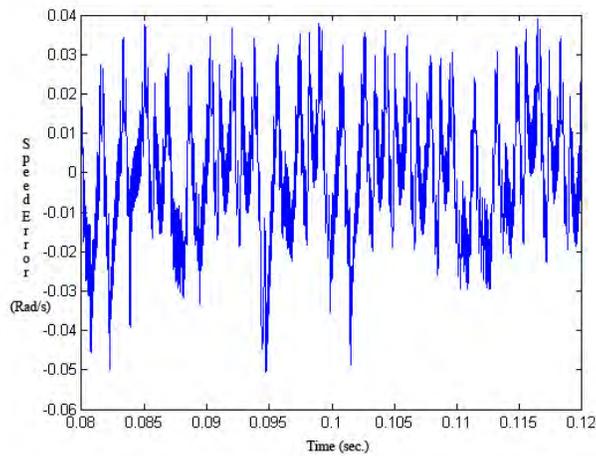

Figure 5.27 Speed Error with Hysteresis Control at 600 rad/s

Figure 5.27 shows the speed error plot for hysteresis control. The drive speed loop operates to maintain the command speed within an error represented in the speed error plot.

The above plots have been repeated with PWM control for comparing hysteresis control with PWM control.

PWM Current Control
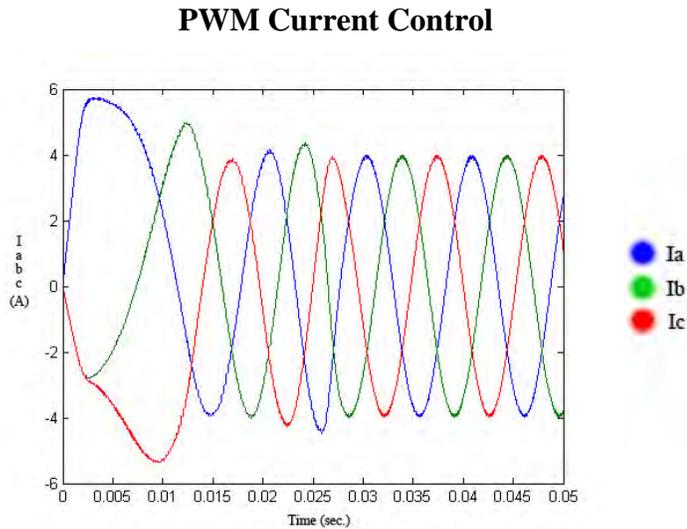
Figure 5.28 Iabc Current with PWM Control at 600 rad/s

Figure 5.28 shows the three phase currents as a result of the PWM current control obtained from Park's reverse transformation. It is clear that the current is non sinusoidal at the starting and becomes sinusoidal when the motor reaches the controller command speed at steady state. The corresponding dq component of current is given in figure 5.29. Both d and q axis current are present. However the q axis current is very small since the torque gets very much reduced at this higher speed due to power being maintained constant.
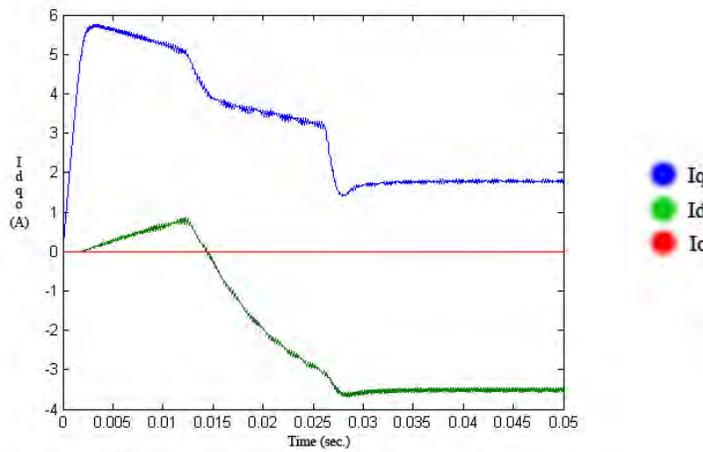
Figure 5.29 Idqo Currents with PWM Control at 600 rad/s
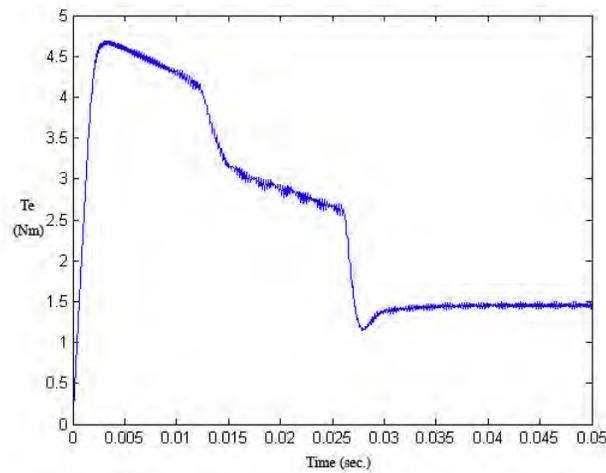
Figure 5.30 Developed Torque with PWM Control at 600 rad/s

Figure 5.30 shows the developed torque of the motor. When the speed of the motor is less than the rated speed, the torque is more and gets reduced at speeds greater than the rated speed.
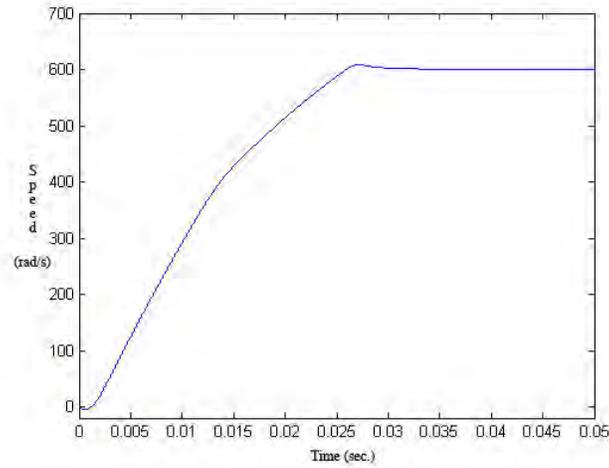
Figure 5.31 Motor Electrical Speed with PWM Control at 600 rad/s

Figure 5.31 shows a variation of the speed with time. The steady state speed is the same as that of the commanded reference speed.
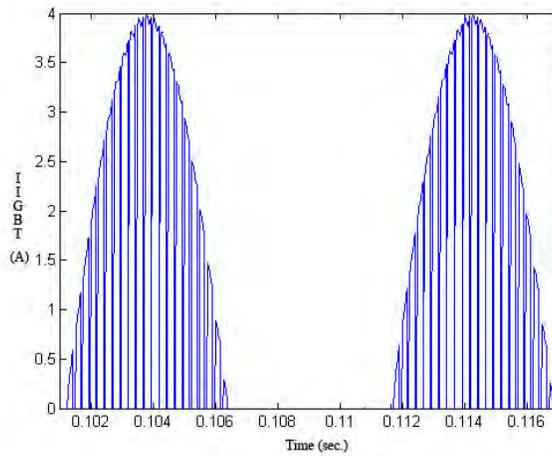
Figure 5.32 IGBT Current with PWM Control at 600 rad/s

Figure 5.32 presents the waveform of the current flowing through the IGBT. The current pulses are similar since the switching frequency is constant.

71
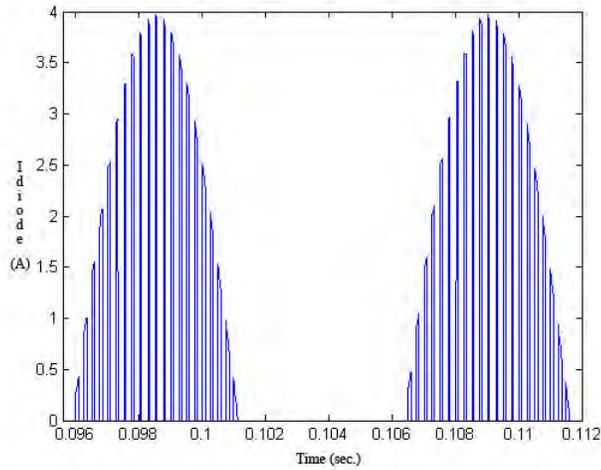
Figure 5.33 Diode Current with PWM Control at 600 rad/s

Figure 5.33 shows the waveform of the current flowing through the antiparallel diode.
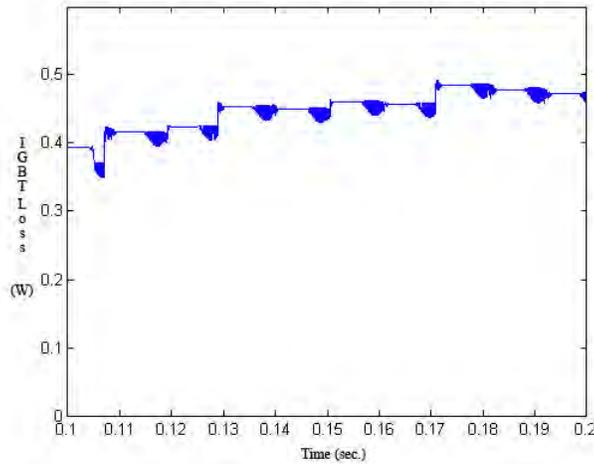
Figure 5.34 IGBT Average Power Loss with PWM Control at 600 rad/s

Figure 5.34 shows the average conduction loss in each IGBT at steady state. The

voltage across the device is multiplied by the current through the device and the average is

taken.
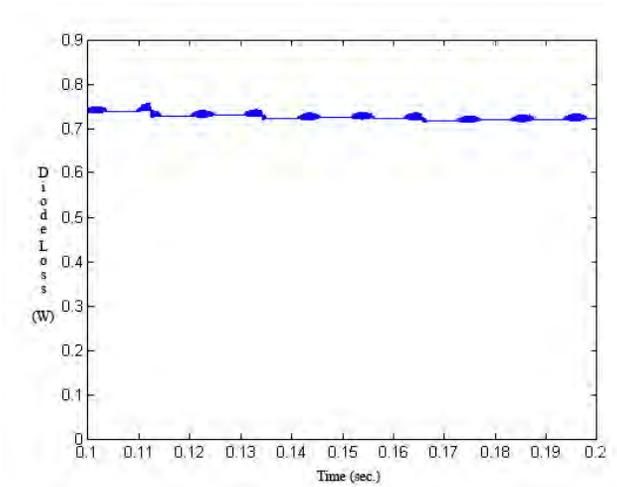
Figure 5.35 Diode Average Power Loss with PWM Control at 600 rad/s

Figure 5.35 shows the average power loss in the diode.
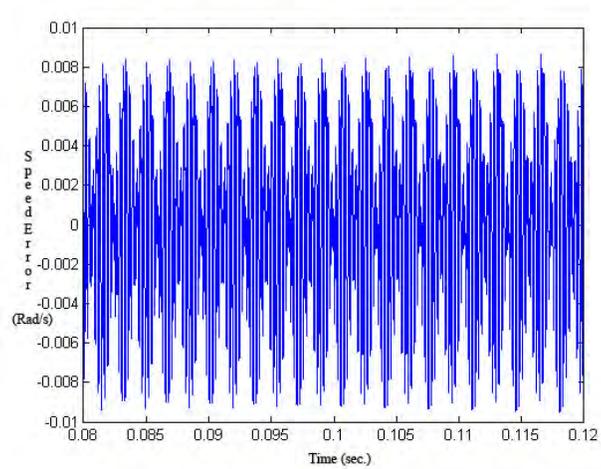
Figure 5.36 Speed Error with PWM Control at 600 rad/s

Figure 5.36 shows the speed error plot for PWM control. The drive speed loop operates to maintain the command speed within an error represented in the speed error plot. The speed error is practically zero with PWM control.

5.1.3 Harmonic Spectrum and Total Harmonic Distortion

Harmonic content in a voltage or current wave form determines the quality of power. The power quality is judged by a factor called Total Harmonic Distortion (THD). The higher the THD the lower is the power quality. The THD can be calculated using equation 5.1.

$$THD\% = \sqrt{\frac{Sum\_of\_all\_squares\_of\_amplitude\_of\_all\_harmonic\_voltages}{Square\_of\_the\_amplitude\_of\_the\_fundamental\_voltage}} \cdot 100\% \qquad \textbf{5.1}$$

Harmonic contents in phase voltages and currents are determined using Fast Fourier Transform (FFT). The results are given below for Hysteresis and PWM modes of current control. These results are obtained using Simulink FFT tool of Powergui to display the frequency spectrum of voltage and current waveforms and THD content. These signals are stored in the workspace in the ASM structure with time variable generated by the Scope block. Because the model is discretized, the signal saved in this structure is sampled at a fixed step and consequently satisfies the FFT tool requirements.

IEEE Standard 519-1992 provides a guideline for the acceptable levels of voltage distortion to loads (including motors). A broad recommendation is to establish the voltage distortion monitoring limits at 5% THD and at 3% for any particular harmonic frequency.

74
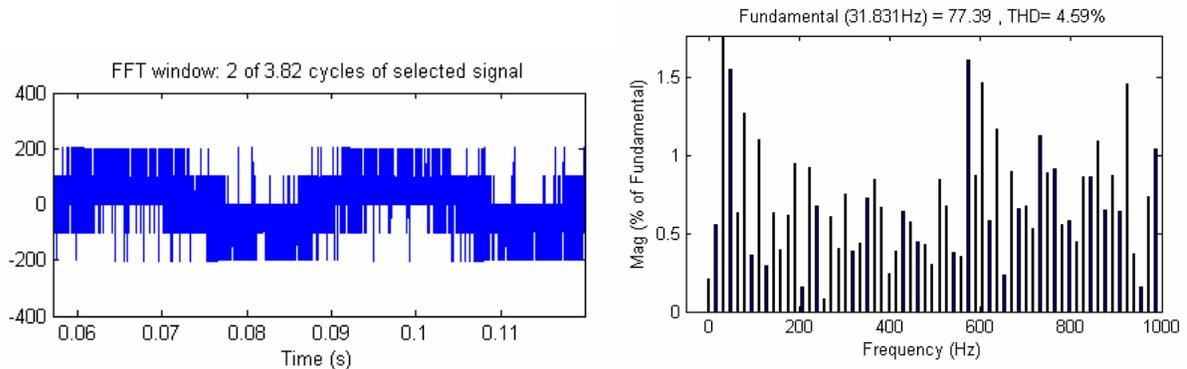
Figure 5.37 Phase Voltage FFT with Hysteresis Control at 200 rad/s

Figure 5.37 shows the phase voltage waveform with hysteresis control and the corresponding harmonic spectrum. The value of THD calculated using Simulink is 4.59% and meets IEEE 519 limits.
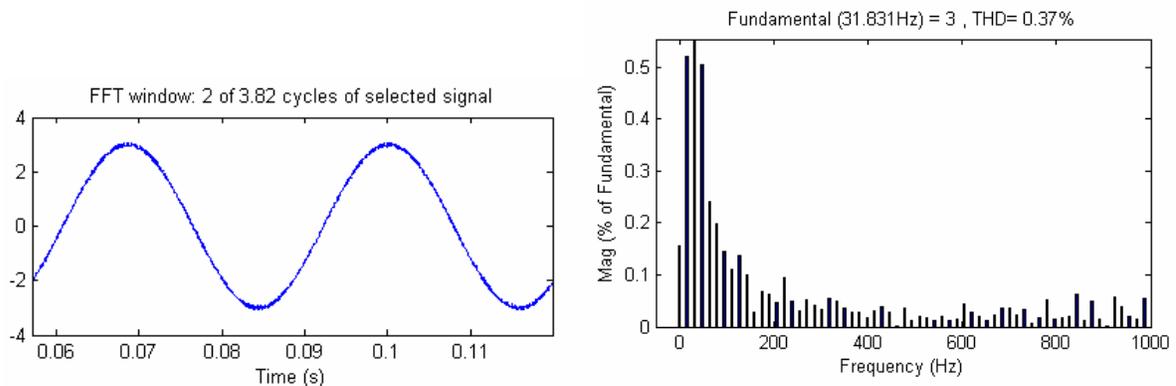

Figure 5.38 Phase Current FFT with Hysteresis Control at 200 rad/s

Figure 5.38 shows the phase current waveform with hysteresis control and the corresponding harmonic spectrum. The value of THD is 0.37%. The current waveform is practicaly sinusoidal because the motor behaves as a filter for higher harmonics.

75
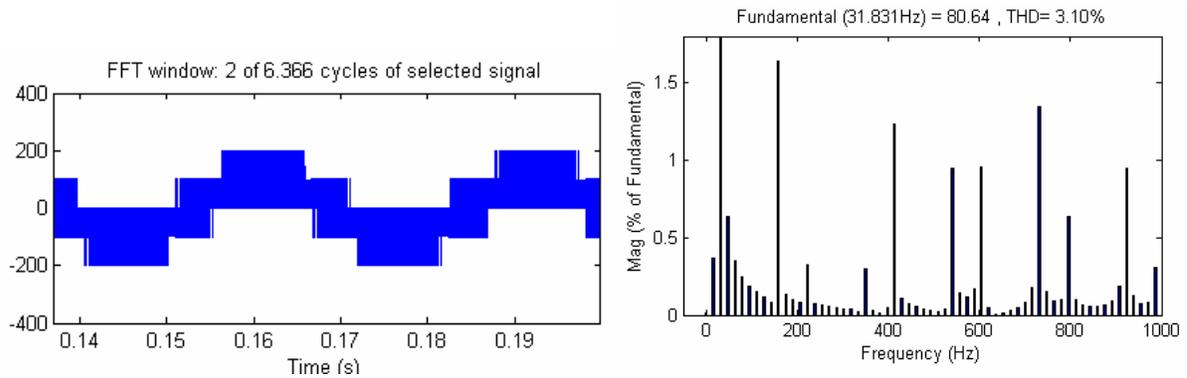
Figure 5.39 Phase Voltage FFT with PWM Control at 200 rad/s

Figure 5.39 shows the phase voltage waveform with PWM control and the corresponding harmonic spectrum. The value of THD calculated using Simulink is 3.10% and meets IEEE 519 limits..
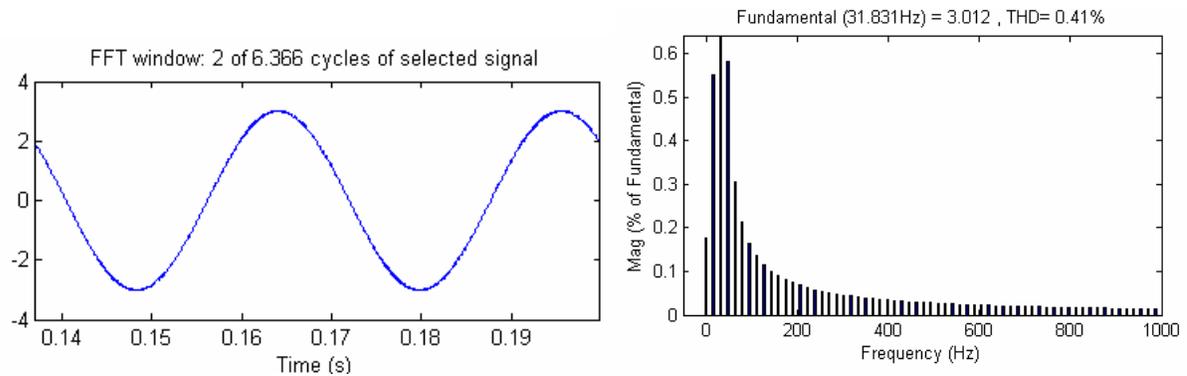

Figure 5.40 Phase Current FFT with PWM Control at 200 rad/s

Figure 5.40 shows the phase current waveform with PWM control and the corresponding harmonic spectrum. The value of THD is 0.41%. Since the motor offers a large impedance to higher harmonic voltages, harmonic currents are practically zero and the current drawn by the motor is sinusoidal.
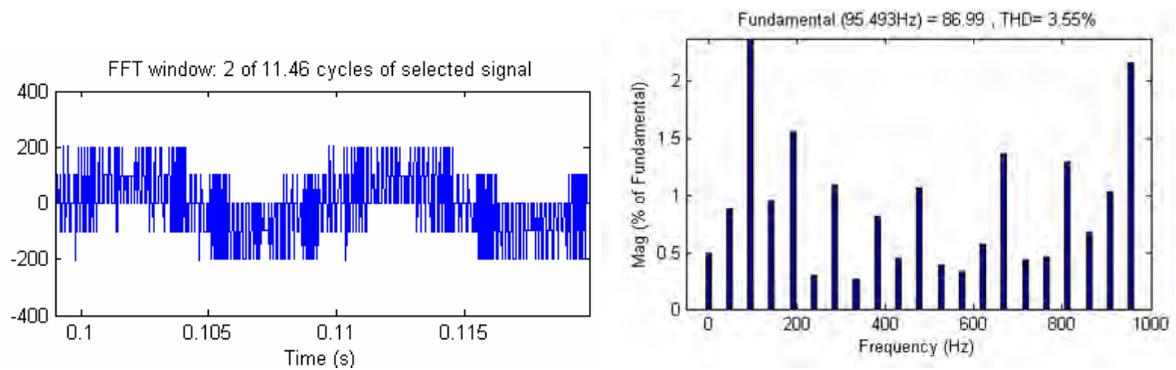
Figure 5.41 Phase Voltage FFT with Hysteresis Control at 600 rad/s

Figure 5.41 shows the phase voltage waveform with hysteresis control and the corresponding harmonic spectrum. The value of THD is 3.55% and meets IEEE 519 limits.
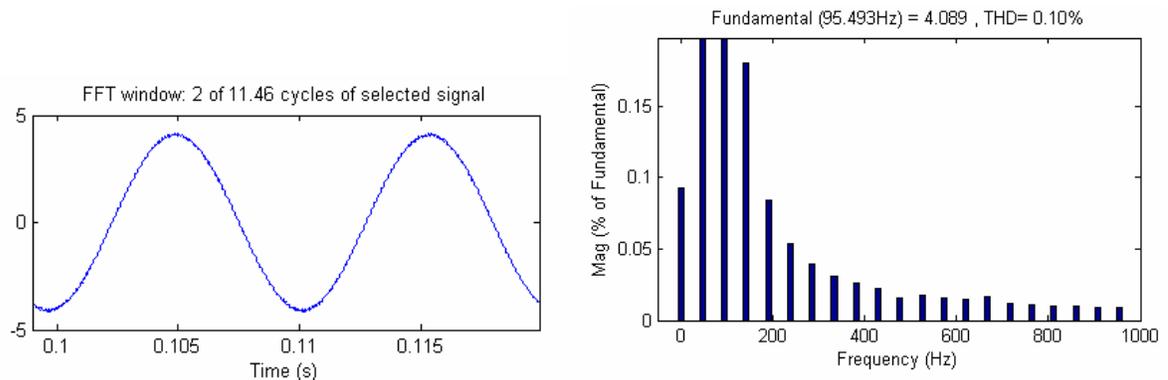
Figure 5.42 Phase Current FFT with Hysteresis Control at 600 rad/s

Figure 5.42 shows the phase Current waveform with hysteresis control and the corresponding harmonic spectrum. The value of THD is 0.10%

77
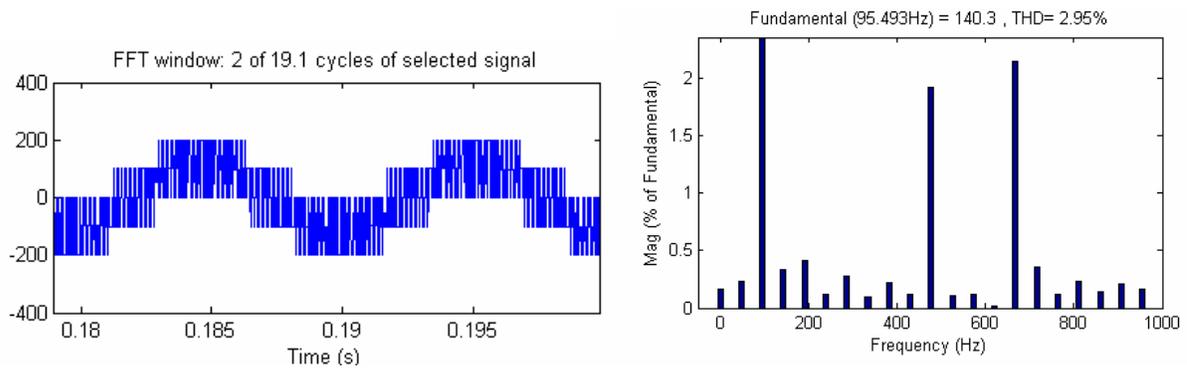
Figure 5.43 Phase Voltage FFT with PWM Control at 600 rad/s

Figure 5.43 shows the phase voltage waveform with PWM control and the

corresponding harmonic spectrum. The value of THD is 2.95% and meets IEEE 519 limits.
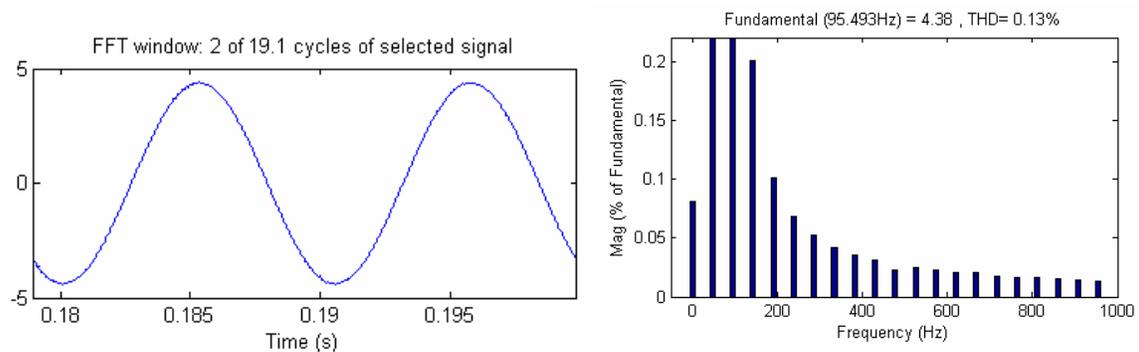
Figure 5.44 Phase Current FFT with PWM Control at 600 rad/s

Figure 5.44 shows the phase current waveform with PWM control and the

corresponding harmonic spectrum. The value of THD is 0.13%

After reviewing the results of the simulation, table 5.2 is prepared which shows the essential points in performance comparison.

Table 5.2 Summary of Results

	Hysteresis 200	PWM 200	Hysteresis 600	PWM 600
Speed Error (rad/s)	0.07	0.016	0.06	0.016
Loss IGBT (w)	0.28	0.28	0.65	0.5
Loss Diode (w)	0.7	0.65	0.9	0.7
Pin (w)	300	330	575	565
Pout (w)	244.8	244.8	436	436
Efficiency	81.6%	74.18%	75.83%	77.17%
Voltage THD%	4.59%	3.10%	3.55%	2.95%
Current THD%	0.37%	0.41%	0.10%	0.13%

The Simulink simulation allows performance study of PM motor drives with two current control techniques. Table 5.2 presents the areas of performance study and detailed simulation results. From the results it is seen that PWM current control technique is superior to hysteresis controller. It is able to maintain the speed error within an extremely small limit. This method also gives lower harmonic contents in motor voltage waveforms. The simulation time with Hysteresis control is short, about 1/3 of the PWM simulation time. Hysteresis control incurs higher switching frequencies with the possibility of exceeding device ratings. PWM has constant switching frequency.

In both methods the voltage THD% is higher than current THD% which demonstrates that the motor acts like a filter for the high order harmonics (low pass filter) that were attenuated by the motor inductances. The voltage and currents THD% for both methods where within IEEE 519 recommended limits.

6 CONCLUSIONS AND FUTURE WORK

6.1 Conclusion

A detailed Simulink model for a PMSM drive system with field oriented control has being developed and operation below and above rated speed has been studied using two current control schemes. Simulink has been chosen from several simulation tools because its flexibility in working with analog and digital devices. Mathematical models can be easily incorporated in the simulation and the presence of numerous tool boxes and support guides simplifies the simulation of large system compared to Spice. Simulink is capable of showing real time results with reduced simulation time and debugging.

In the present simulation measurement of currents and voltages in each part of the system is possible, thus permitting the calculation of instantaneous or average losses, efficiency of the drive system and total harmonic distortion.

Usually in such a drive system the inverter is driven either by hysteresis or by PWM current controllers. A comparative study has been made of the two current control schemes in terms of switching frequency, device losses, power quality, speed error and current control ability. This study proves that PWM current controllers are better than hysteresis current controllers because of having constant switching frequency and lower THD of the input voltage waveforms. The error between the speed command and the actual speed is also greatly reduced. Hysteresis current controllers have a variable switching frequency that depends of the hysteresis band and if the bandwidth is very small it may affect the device

switching capability. However, the simulation with hysteresis current controller allows faster simulations with reduced time and computational resources.

A speed controller has been designed successfully for closed loop operation of the PMSM drive system so that the motor runs at the commanded or reference speed. The simulated system has a fast response with practically zero steady state error thus validating the design method of the speed controller.

6.2 Future Work

The implementation of additional control techniques like unity power factor control, constant mutual air gap flux linkages control, optimum torque per ampere control and sensor-less control can be taken up for detail simulation and performance calculation of PMSM drive systems. Detailed modeling and simulation of other types of synchronous motor drives can also be taken up for transient and steady state analysis.

REFERENCES

[1]   T. Sebastian, G. Slemon, and M. Rahman, "Modelling of permanent magnet synchronous motors," *Magnetics, IEEE Transactions on*, vol. 22, pp. 1069-1071, 1986.

[2]   T. M. Jahns, G. B.Kliman, and T. W. Neumann, "Interior Permanent-Magnet Synchronous Motors for Adjustable-Speed Drives," *Industrial Applications, IEEE Transactions on*, vol. IA-22, pp. 738-746, 1986.

[3]   P. Pillay and R. Krishnan, "Modeling of permanent magnet motor drives," *Industrial Electronics, IEEE Transactions on*, vol. 35, pp. 537-541, 1988.

[4]   P. Pillay and R. Krishnan, "Modeling, simulation, and analysis of permanent-magnet motor drives. I. The permanent-magnet synchronous motor drive," *Industry Applications, IEEE Transactions on*, vol. 25, pp. 265-273, 1989.

[5]   S. Morimoto, Y. Tong, Y. Takeda, and T. Hirasa, "Loss minimization control of permanent magnet synchronous motor drives," *Industrial Electronics, IEEE Transactions on*, vol. 41, pp. 511-517, 1994.

[6]   A. H. Wijenayake and P. B. Schmidt, "Modeling and analysis of permanent magnet synchronous motor by taking saturation and core loss into account," 1997.

[7]   K. Jang-Mok and S. Seung-Ki, "Speed control of interior permanent magnet synchronous motor drive for the flux weakening operation," *Industry Applications, IEEE Transactions on*, vol. 33, pp. 43-48, 1997.

[8]   B. K. Bose, *Modern power electronics and AC drives*: Prentice Hall, 2002.

[9]   B. Cui, J. Zhou, and Z. Ren, "Modeling and simulation of permanent magnet synchronous motor drives," 2001.

[10]   C. Mademlis and N. Margaris, "Loss minimization in vector-controlled interior permanent-magnet synchronous motor drives," *Industrial Electronics, IEEE Transactions on*, vol. 49, pp. 1344-1347, 2002.

[11]   X. Jian-Xin, S. K. Panda, P. Ya-Jun, L. Tong Heng, and B. H. Lam, "A modular control scheme for PMSM speed control with pulsating torque minimization," *Industrial Electronics, IEEE Transactions on*, vol. 51, pp. 526-536, 2004.

[12]   R. E. Araujo, A. V. Leite, and D. S. Freitas, "The Vector Control Signal Processing blockset for use with Matlab and Simulink," 1997.

[13]   C.-m. Ong, *Dynamic Simulation of Electric Machinery using Matlab/Simulink*: Prentice Hall, 1998.

[14]   H. Macbahi, A. Ba-razzouk, J. Xu, A. Cheriti, and V. Rajagopalan, "A unified method for modeling and simulation of three phase induction motor drives," 2000.

[15]   J. H. Reece, C. W. Bray, J. J. Van Tol, and P. K. Lim, "Simulation of power systems containing adjustable speed drives," 1997.

[16]   C. D. French, J. W. Finch, and P. P. Acarnley, "Rapid prototyping of a real time DSP based motor drive controller using Simulink," 1998.

[17]   S. Onoda and A. Emadi, "PSIM-based modeling of automotive power systems: conventional, electric, and hybrid electric vehicles," *Vehicular Technology, IEEE Transactions on*, vol. 53, pp. 390-400, 2004.

[18]   G. Venkaterama, "Simulink Permanent Magnet Simulation," *University of Wisconsin*.

[19]   Mathlab-Works-Support, "PM Synchronous Motor Drive," *http://www.mathworks.com/access/helpdesk/help/toolbox/physmod/powersys/powersys.html*.

[20]   Mathlab-Works-Support, "PM Synchronous Motor," *http://www.mathworks.com/access/helpdesk/help/toolbox/physmod/powersys/powersys.html*.

[21]   M. Aydin, "Axial Flux Mounted Permanent Magnet Disk Motors For Smooth Torque Traction Drive Application," in *Electrical and Computer Engineering*, vol. PhD: University of Wisconsin 2004, pp. 453.

[22]   R. Krishnan, *Electric Motor Drives Modeling, Analysis, and Control* Pearson Education, 2001.

[23]   B. K. Bose, *Power Electronics and Variable Frequency Drives*, 1 ed: Wiley, John & Sons, 1996.

[24]   National-Instruments, "Optical Encoder Fundamentals," http://zone.ni.com/devzone%5Cconceptd.nsf/webmain/73304E4E321EF5EA86256B3500782979?opendocument.

[25]   National-Instruments, "Quadrature Encoder Fundamentals," http://zone.ni.com/devzone%5Cconceptd.nsf/webmain/665470207873076386256B35007957A2?opendocument.

[26]   BEI-TECHNOLOGIES, "Optical Encoder Design," http://www.beiied.com/PDFs2/Optical_Encoder_Design.pdf.

[27]   Freescale-Semiconductor, "AN1943 56F80x Resolver Driver and Hardware Interface," http://www.freescale.com/files/product/doc/AN1942.pdf, 2005.

[28]   X. Junfeng, W. Fengyan, F. Jianghua, and X. Jianping, "Flux-weakening control of permanent magnet synchronous motor with direct torque control consideration variation of parameters," 2004.

APPENDIX 1

International IQR Rectifier

PD-94576A

IRGIB10B60KD1

INSULATED GATE BIPOLAR TRANSISTOR WITH
ULTRAFAST SOFT RECOVERY DIODE

Features
- Low VCE (on) Non Punch Through IGBT Technology.
- Low Diode VF.
- 10µs Short Circuit Capability.
- Square RBSOA.
- Ultrasoft Diode Reverse Recovery Characteristics.
- Positive VCE (on) Temperature Coefficient.
- Maximum Junction Temperature Rated at 175°C

Benefits
- Benchmark Efficiency for Motor Control.
- Rugged Transient Performance.
- Low EMI.
- Excellent Current Sharing in Parallel Operation.

n-channel

$V_{CES} = 600V$

$I_C = 10A, T_C = 100°C$

$t_{sc} > 10µs, T_J = 150°C$

$V_{CE(on)}$ typ. $= 1.7V$

TO-220
Full-Pak
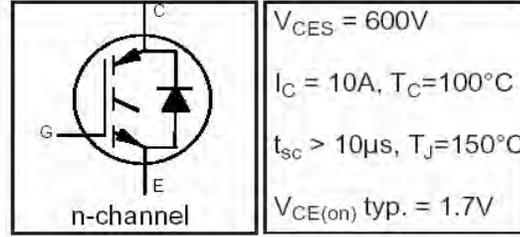
Absolute Maximum Ratings

	Parameter	Max.	Units
V_{CES}	Collector-to-Emitter Voltage	600	V
I_C @ T_C = 25°C	Continuous Collector Current	16	
I_C @ T_C = 100°C	Continuous Collector Current	10	A
I_{CM}	Pulse Collector Current (Ref.Fig.C.T.5)	32	
I_{LM}	Clamped Inductive Load current ①	32	
I_F @ T_C = 25°C	Diode Continuous Forward Current	16	
I_F @ T_C = 100°C	Diode Continuous Forward Current	10	
I_{FM}	Diode Maximum Forward Current	32	
V_{ISOL}	RMS Isolation Voltage, Terminal to Case, t = 1 min	2500	V
V_{GE}	Gate-to-Emitter Voltage	±20	
P_D @ T_C = 25°C	Maximum Power Dissipation	44	W
P_D @ T_C = 100°C	Maximum Power Dissipation	22	
T_J	Operating Junction and	-55 to +175	
T_{STG}	Storage Temperature Range		°C
	Soldering Temperature for 10 sec.	300 (0.063 in. (1.6mm) from case)	
	Mounting Torque, 6-32 or M3 Screw	10 lbf.in (1.1N.m)	

Thermal / Mechanical Characteristics

	Parameter	Min.	Typ.	Max.	Units
$R_{\theta JC}$	Junction-to-Case- IGBT	——	——	3.4	
$R_{\theta JC}$	Junction-to-Case- Diode	——	——	5.3	°C/W
$R_{\theta CS}$	Case-to-Sink, flat, greased surface	——	0.50	——	
$R_{\theta JA}$	Junction-to-Ambient, typical socket mount	——	——	62	
Wt	Weight	——	2.0	——	g

www.irf.com

1

2/27/04

IRGIB10B60KD1

Electrical Characteristics @ T$_J$ = 25°C (unless otherwise specified)

	Parameter	Min.	Typ.	Max.	Units	Conditions
V$_{(BR)CES}$	Collector-to-Emitter Breakdown Voltage	600	—	—	V	V$_{GE}$ = 0V, I$_C$ = 500µA
ΔV$_{(BR)CES}$/ΔT$_J$	Temperature Coeff. of Breakdown Voltage	—	0.99	—	V/°C	V$_{GE}$ = 0V, I$_C$ = 1mA (25°C-150°C)
V$_{CE(on)}$	Collector-to-Emitter Voltage	1.50	1.70	2.10	V	I$_C$ = 10A, V$_{GE}$ = 15V, T$_J$ = 25°C
		—	2.05	2.35		I$_C$ = 10A, V$_{GE}$ = 15V, T$_J$ = 150°C
		—	2.06	2.35		I$_C$ = 10A, V$_{GE}$ = 15V, T$_J$ = 175°C
V$_{GE(th)}$	Gate Threshold Voltage	3.5	4.5	5.5	V	V$_{CE}$ = V$_{GE}$, I$_C$ = 250µA
ΔV$_{GE(th)}$/ΔT$_J$	Threshold Voltage temp. coefficient	—	-10	—	mV/°C	V$_{CE}$ = V$_{GE}$, I$_C$ = 1mA (25°C-150°C)
gfe	Forward Transconductance	—	5.0	—	S	V$_{CE}$ = 50V, I$_C$ = 10A, PW = 80µs
I$_{CES}$	Zero Gate Voltage Collector Current	—	1.0	150	µA	V$_{GE}$ = 0V, V$_{CE}$ = 600V
		—	90	250		V$_{GE}$ = 0V, V$_{CE}$ = 600V, T$_J$ = 150°C
		—	150	400		V$_{GE}$ = 0V, V$_{CE}$ = 600V, T$_J$ = 175°C
V$_{FM}$	Diode Forward Voltage Drop	—	1.80	2.40	V	I$_F$ = 5.0A, V$_{GE}$ = 0V
		—	1.32	1.74		I$_F$ = 5.0A, V$_{GE}$ = 0V, T$_J$ = 150°C
		—	1.23	1.62		I$_F$ = 5.0A, V$_{GE}$ = 0V, T$_J$ = 175°C
I$_{GES}$	Gate-to-Emitter Leakage Current	—	—	±100	nA	V$_{GE}$ = ±20V, V$_{CE}$ = 0V

Switching Characteristics @ T$_J$ = 25°C (unless otherwise specified)

	Parameter	Min.	Typ.	Max.	Units	Conditions
Q$_g$	Total Gate Charge (turn-on)	—	41	62		I$_C$ = 10A
Q$_{ge}$	Gate-to-Emitter Charge (turn-on)	—	4.6	6.9	nC	V$_{CC}$ = 400V
Q$_{gc}$	Gate-to-Collector Charge (turn-on)	—	19	29		V$_{GE}$ = 15V
E$_{on}$	Turn-On Switching Loss	—	156	264		I$_C$ = 10A, V$_{CC}$ = 400V
E$_{off}$	Turn-Off Switching Loss	—	165	273	µJ	V$_{GE}$ = 15V, R$_G$ = 50Ω, L = 1.07mH
E$_{tot}$	Total Switching Loss	—	321	434		Ls= 150nH, T$_J$ = 25°C ②
t$_{d(on)}$	Turn-On delay time	—	25	33		I$_C$ = 10A, V$_{CC}$ = 400V
t$_r$	Rise time	—	24	34	ns	V$_{GE}$ = 15V, R$_G$ = 50Ω, L = 1.1mH
t$_{d(off)}$	Turn-Off delay time	—	180	250		Ls= 150nH, T$_J$ = 25°C
t$_f$	Fall time	—	62	87		
E$_{on}$	Turn-On Switching Loss	—	261	372		I$_C$ = 10A, V$_{CC}$ = 400V
E$_{off}$	Turn-Off Switching Loss	—	313	425	µJ	V$_{GE}$ = 15V, R$_G$ = 50Ω, L = 1.07mH
E$_{tot}$	Total Switching Loss	—	574	694		Ls= 150nH, T$_J$ = 150°C ②
t$_{d(on)}$	Turn-On delay time	—	22	31		I$_C$ = 8.0A, V$_{CC}$ = 400V
t$_r$	Rise time	—	24	34	ns	V$_{GE}$ = 15V, R$_G$ = 50Ω, L = 1.07mH
t$_{d(off)}$	Turn-Off delay time	—	240	340		Ls= 150nH, T$_J$ = 150°C
t$_f$	Fall time	—	48	67		
L$_E$	Internal Emitter Inductance	—	7.5	—	nH	Measured 5 mm from package
C$_{ies}$	Input Capacitance	—	610	915		V$_{GE}$ = 0V
C$_{oes}$	Output Capacitance	—	66	99	pF	V$_{CC}$ = 30V
C$_{res}$	Reverse Transfer Capacitance	—	23	35		f = 1.0MHz
RBSOA	Reverse Bias Safe Operating Area	FULL SQUARE				T$_J$ = 150°C, I$_C$ = 32A, Vp = 600V V$_{CC}$=500V,V$_{GE}$ = +15V to 0V,R$_G$ = 50Ω
SCSOA	Short Circuit Safe Operating Area	10	—	—	µs	T$_J$ = 150°C, Vp = 600V, R$_G$ = 50Ω V$_{CC}$=360V,V$_{GE}$ = +15V to 0V
I$_{SC (PEAK)}$	Peak Short Circuit Collector Current	—	100	—	A	
E$_{rec}$	Reverse Recovery Energy of the Diode	—	99	128	µJ	T$_J$ = 150°C
t$_{rr}$	Diode Reverse Recovery Time	—	79	103	ns	V$_{CC}$ = 400V, I$_F$ = 10A, L = 1.07mH
I$_{rr}$	Peak Reverse Recovery Current	—	14	18	A	V$_{GE}$ = 15V, R$_G$ = 50Ω
Q$_{rr}$	Diode Reverse Recovery Charge	—	553	719	nC	di/dt = 500A/µs

① Vcc =80% (V$_{CES}$), V$_{GE}$ = 20V, L =100µH, R$_G$ = 50Ω.   ② Energy losses include "tail" and diode reverse recovery.

2

IRGIB10B60KD1
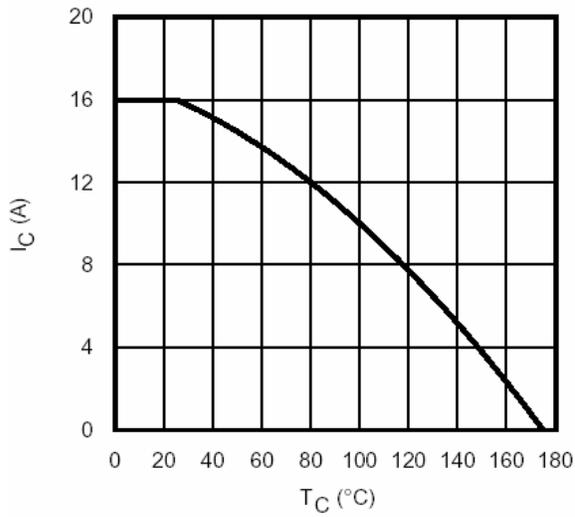

Fig. 1 - Maximum DC Collector Current vs. Case Temperature
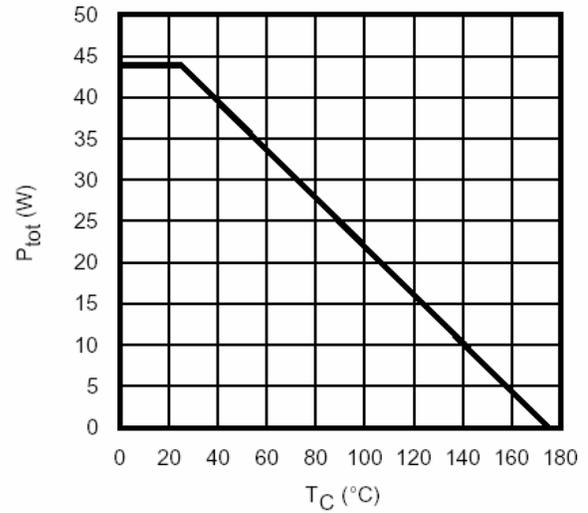
Fig. 2 - Power Dissipation vs. Case Temperature
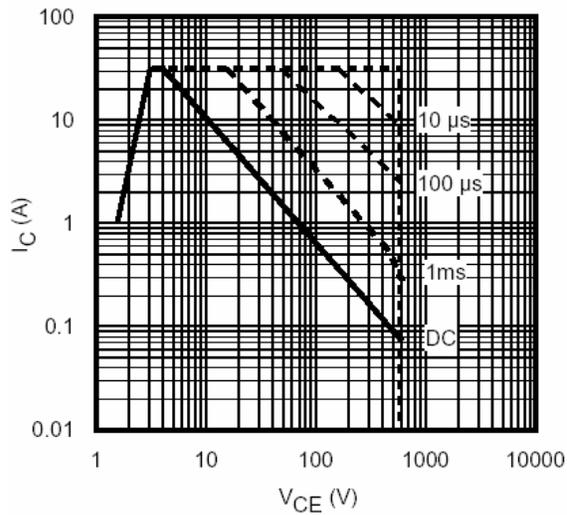

Fig. 3 - Forward SOA
$T_C = 25°C; T_J \le 175°C$
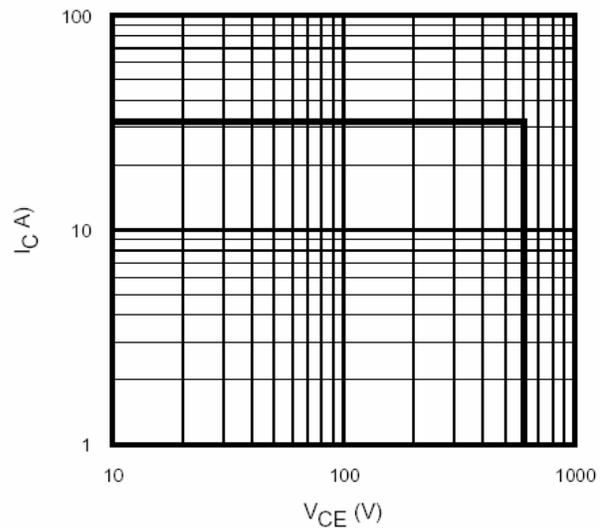
Fig. 4 - Reverse Bias SOA
$T_J = 150°C; V_{GE} = 15V$
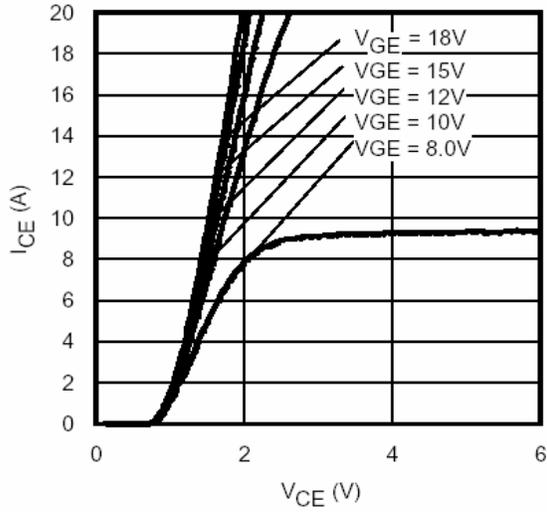
Fig. 5 - Typ. IGBT Output Characteristics
T_J = -40°C; tp = 80µs
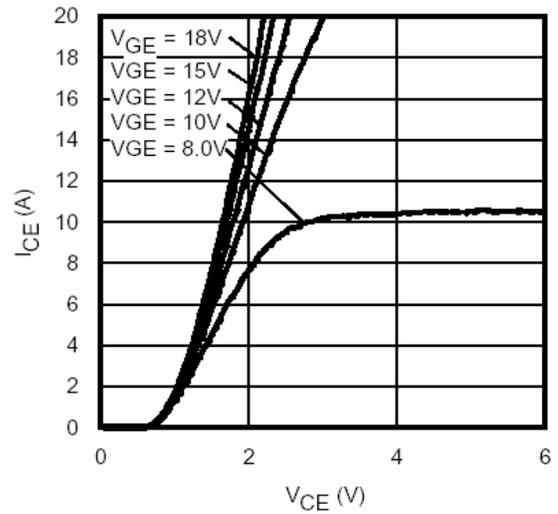
Fig. 6 - Typ. IGBT Output Characteristics
T_J = 25°C; tp = 80µs
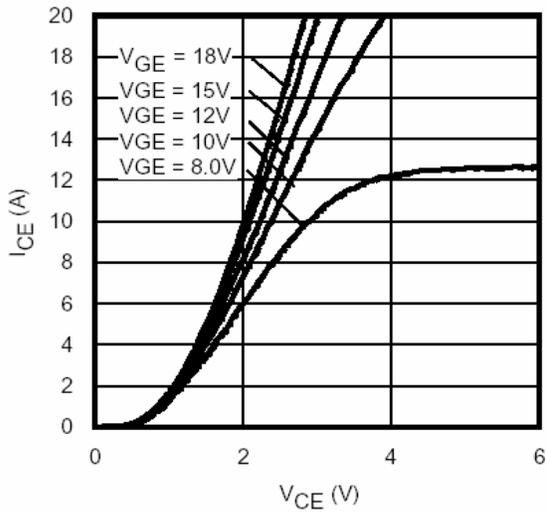
Fig. 7 - Typ. IGBT Output Characteristics
T_J = 150°C; tp = 80µs
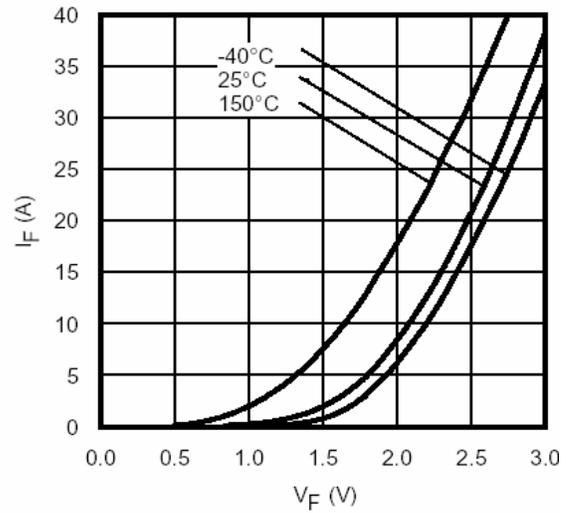
Fig. 8 - Typ. Diode Forward Characteristics
tp = 80µs

4
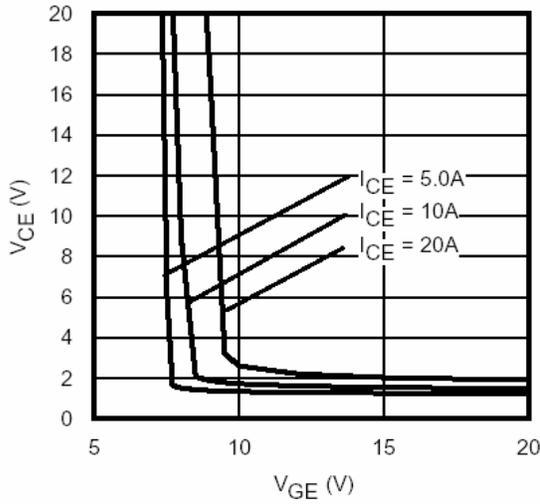
IRGIB10B60KD1

Fig. 9 - Typical V_{CE} vs. V_{GE}
T_J = -40°C
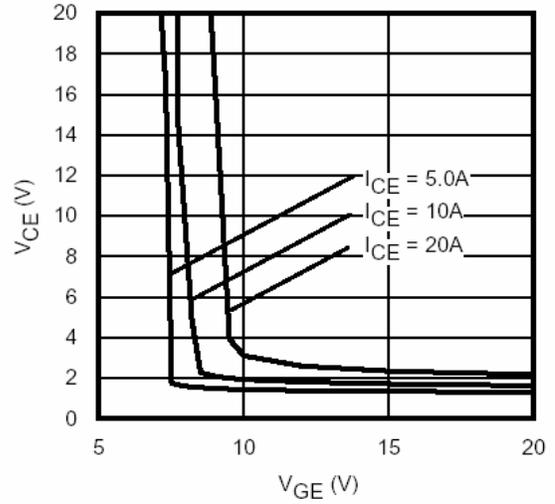
Fig. 10 - Typical V_{CE} vs. V_{GE}
T_J = 25°C
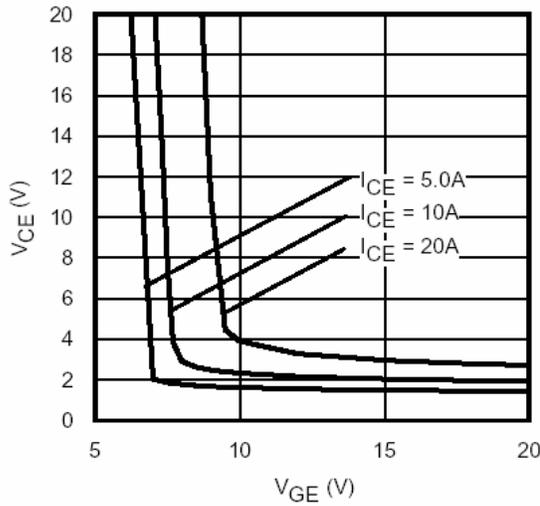
Fig. 11 - Typical V_{CE} vs. V_{GE}
T_J = 150°C
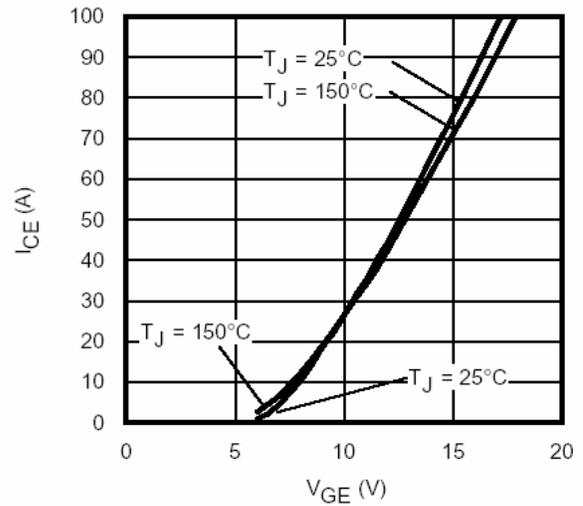
Fig. 12 - Typ. Transfer Characteristics
V_{CE} = 50V; tp = 10µs

IRGIB10B60KD1
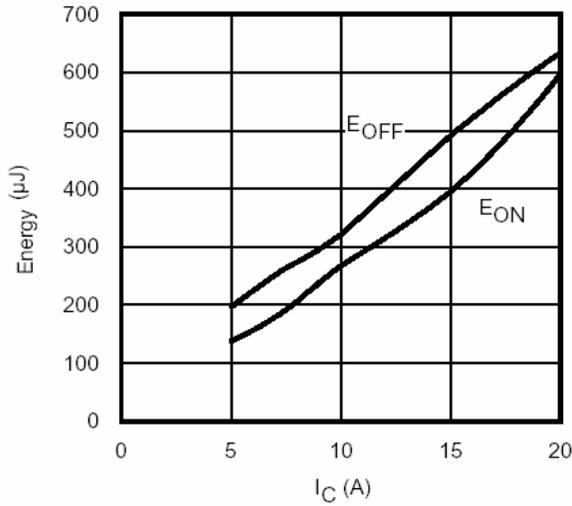
Fig. 13 - Typ. Energy Loss vs. I_C
$T_J = 150°C$; $L=1.07mH$; $V_{CE}= 400V$
$R_G= 50\Omega$; $V_{GE}= 15V$
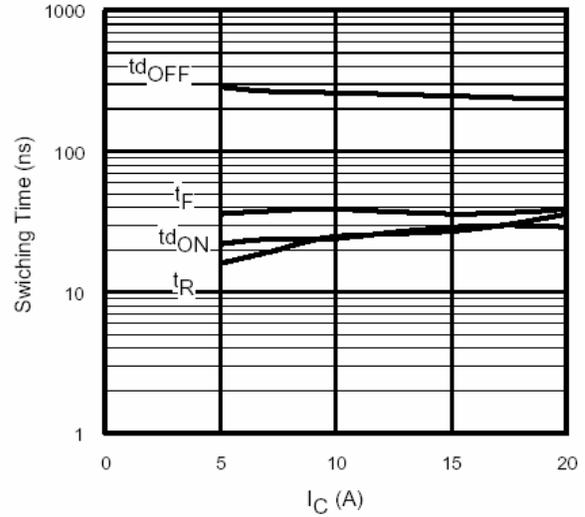
Fig. 14 - Typ. Switching Time vs. I_C
$T_J = 150°C$; $L=1.07mH$; $V_{CE}= 400V$
$R_G= 50\Omega$; $V_{GE}= 15V$
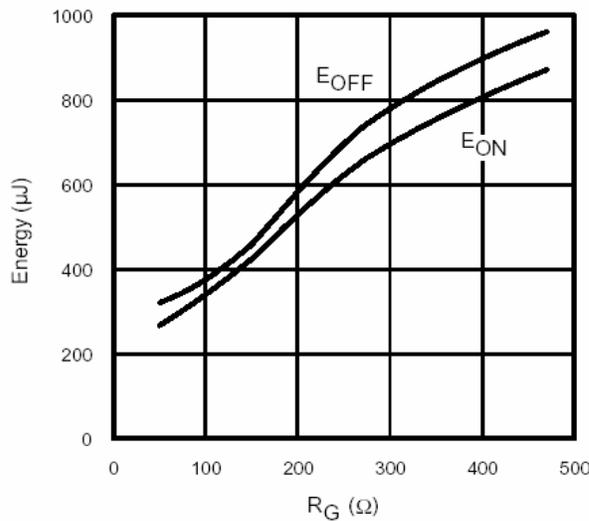
Fig. 15 - Typ. Energy Loss vs. R_G
$T_J = 150°C$; $L=1.07mH$; $V_{CE}= 400V$
$I_{CE}= 10A$; $V_{GE}= 15V$
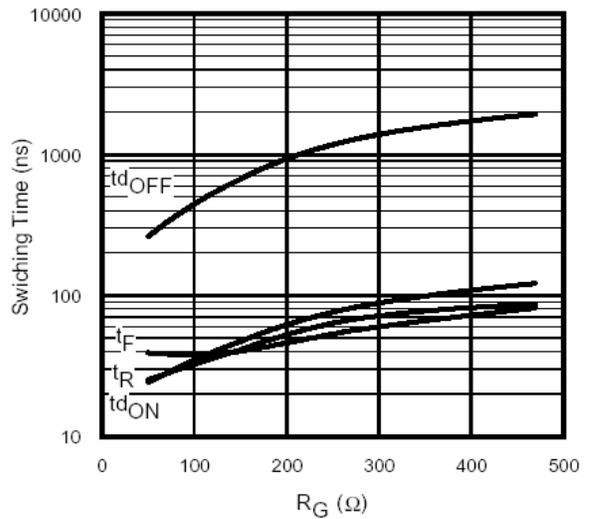
Fig. 16 - Typ. Switching Time vs. R_G
$T_J = 150°C$; $L=1.07mH$; $V_{CE}= 400V$
$I_{CE}= 10A$; $V_{GE}= 15V$

6
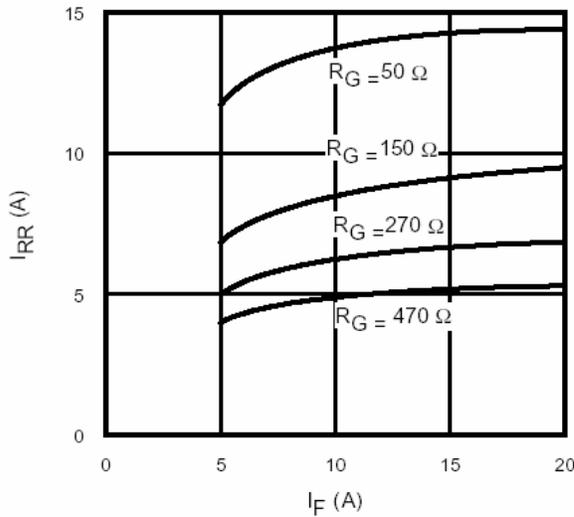
Fig. 17 - Typical Diode I_{RR} vs. I_F
T_J = 150°C
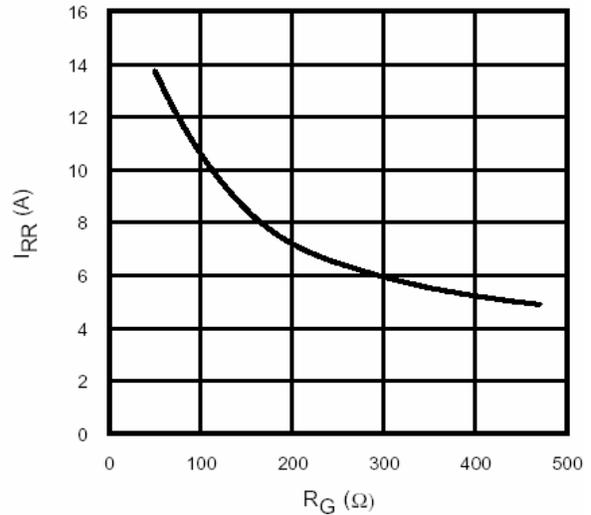
Fig. 18 - Typical Diode I_{RR} vs. R_G
T_J = 150°C; I_F = 10A
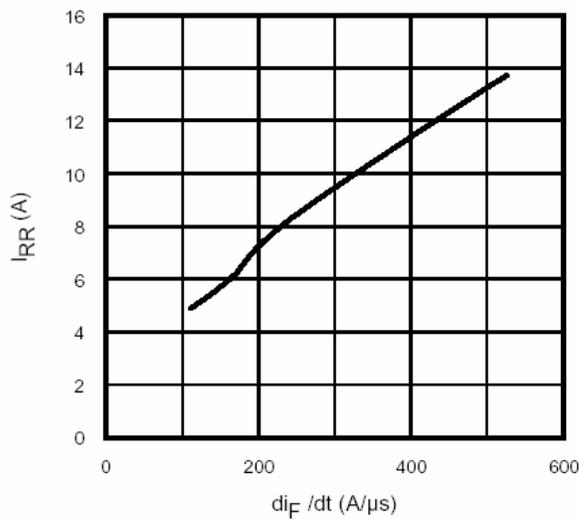
Fig. 19- Typical Diode I_{RR} vs. di_F/dt
V_{CC}= 400V; V_{GE}= 15V;
I_{CE}= 10A; T_J = 150°C
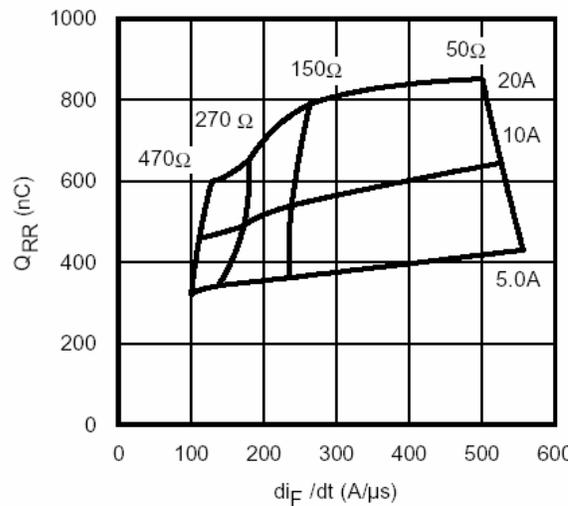
Fig. 20 - Typical Diode Q_{RR}
V_{CC}= 400V; V_{GE}= 15V;T_J = 150°C
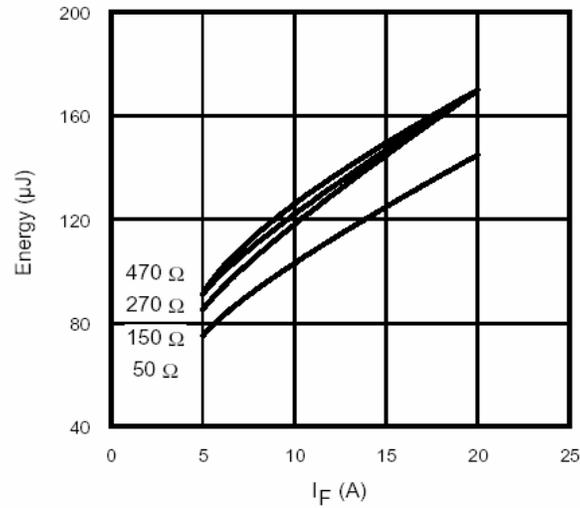
Fig. 21 - Typical Diode E_{RR} vs. I_F
$T_J = 150°C$
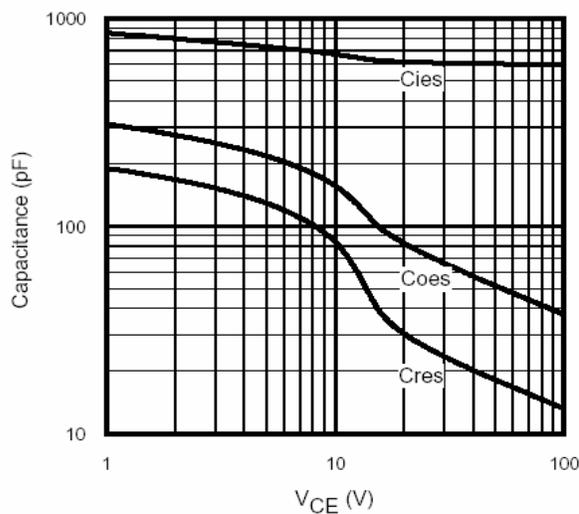
Fig. 22- Typ. Capacitance vs. V_{CE}
$V_{GE}= 0V$; $f = 1MHz$
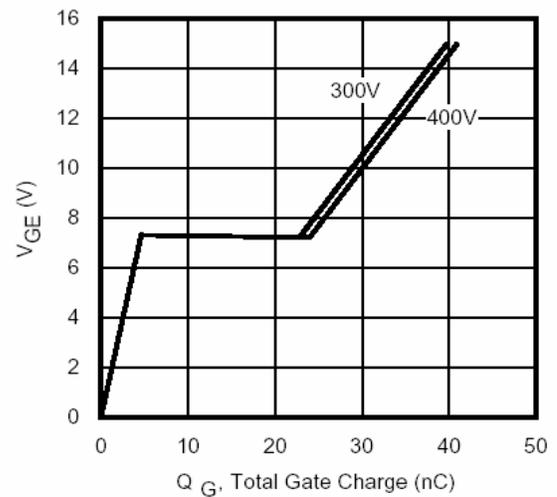
Fig. 23 - Typical Gate Charge vs. V_{GE}
$I_{CE} = 10A$; $L = 2500µH$

8
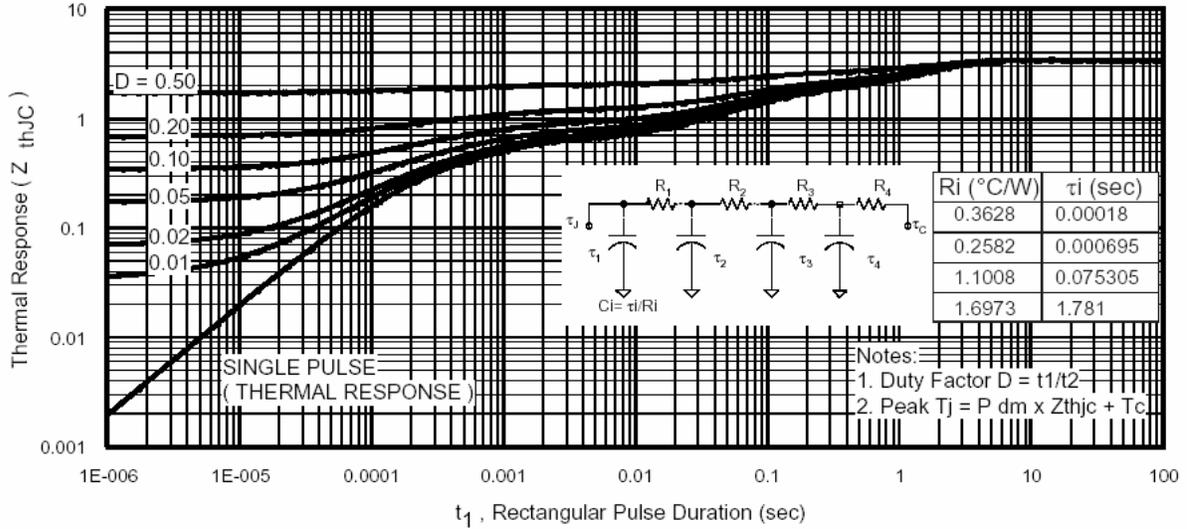
Fig 24. Maximum Transient Thermal Impedance, Junction-to-Case (IGBT)
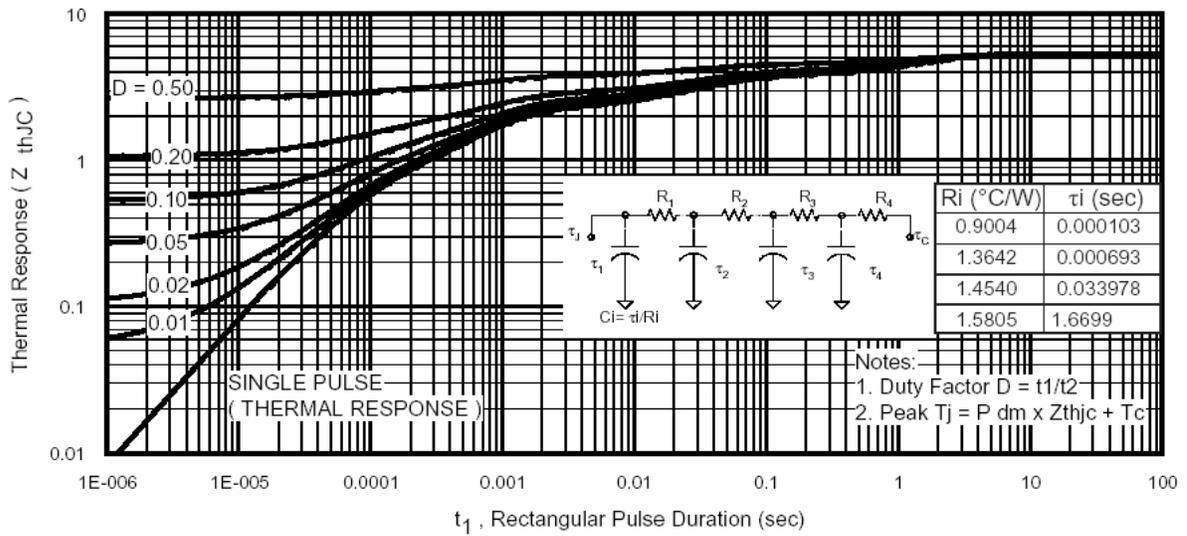
Fig 25. Maximum Transient Thermal Impedance, Junction-to-Case (DIODE)

IRGIB10B60KD1
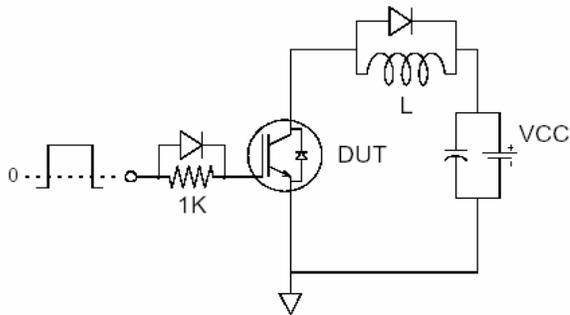
Fig.C.T.1 - Gate Charge Circuit (turn-off)
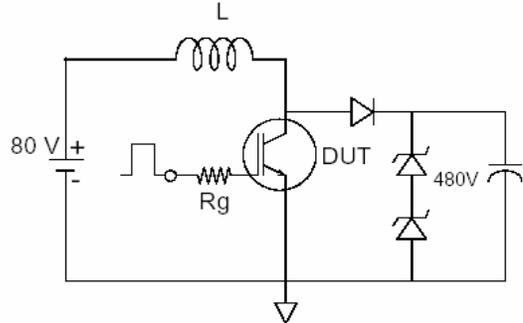
Fig.C.T.2 - RBSOA Circuit
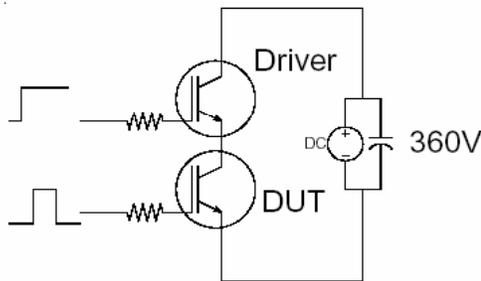
Fig.C.T.3 - S.C.SOA Circuit
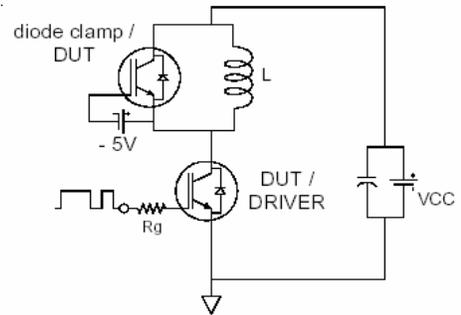
Fig.C.T.4 - Switching Loss Circuit
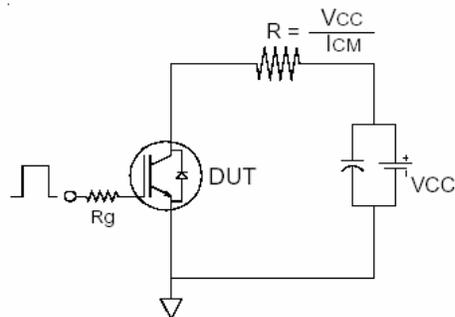

Fig.C.T.5 - Resistive Load Circuit
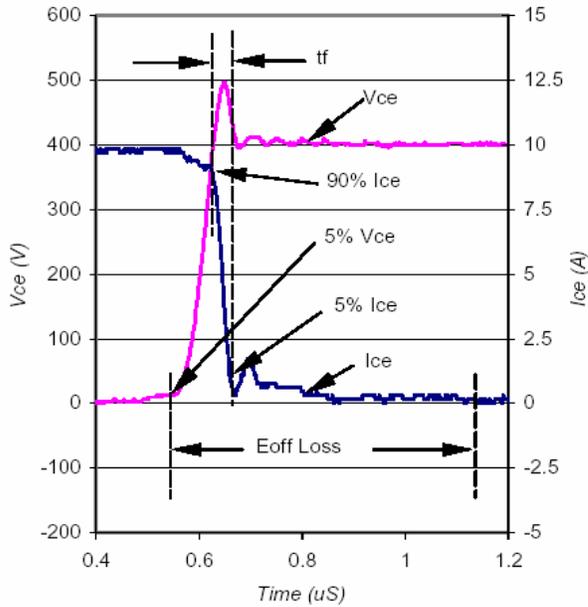
Fig. WF1- Typ. Turn-off Loss Waveform
@ T_J = 150°C using Fig. CT.4
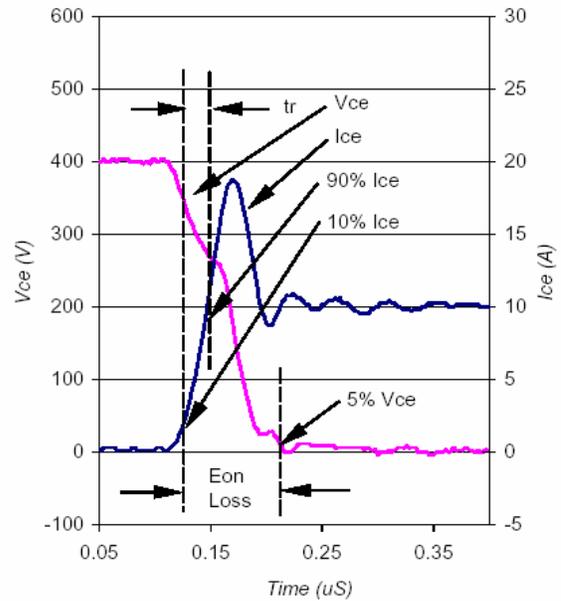
Fig. WF2- Typ. Turn-on Loss Waveform
@ T_J = 150°C using Fig. CT.4
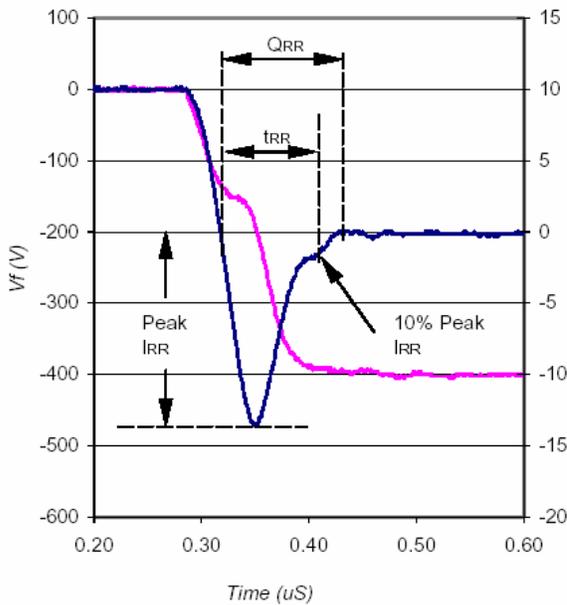

Fig. WF3- Typ. Diode Recovery Waveform
@ T_J = 150°C using Fig. CT.4
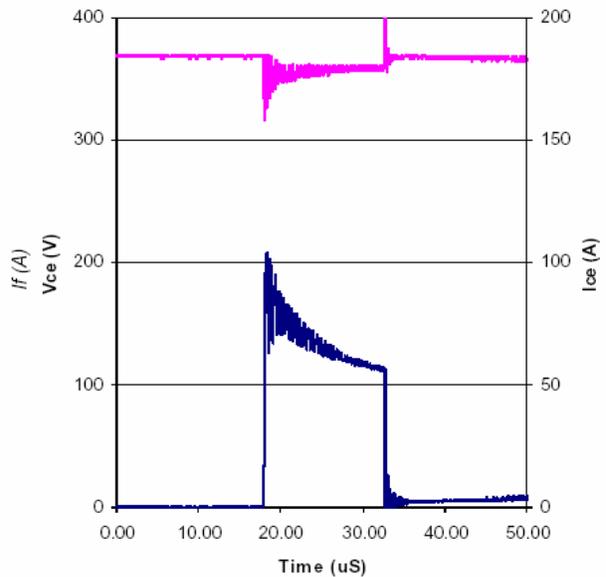
Fig. WF4- Typ. S.C Waveform
@ T_C = 150°C using Fig. CT.3

www.irf.com

11

IRGIB10B60KD1

TO-220 Full-Pak Package Outline
Dimensions are shown in millimeters (inches)

LEAD ASSIGNMENTS

HEXFET	IGBTs, CoPACK
1.- GATE	1.- GATE
2.- DRAIN	2.- COLLECTOR
3.- SOURCE	3.- EMITTER

NOTES:

1 DIMENSIONING & TOLERANCING PER ANSI Y14.5M, 1982

2 CONTROLLING DIMENSION: INCH.

MINIMUM CREEPAGE DISTANCE BETWEEN A-B-C-D = 4.80 (.189)
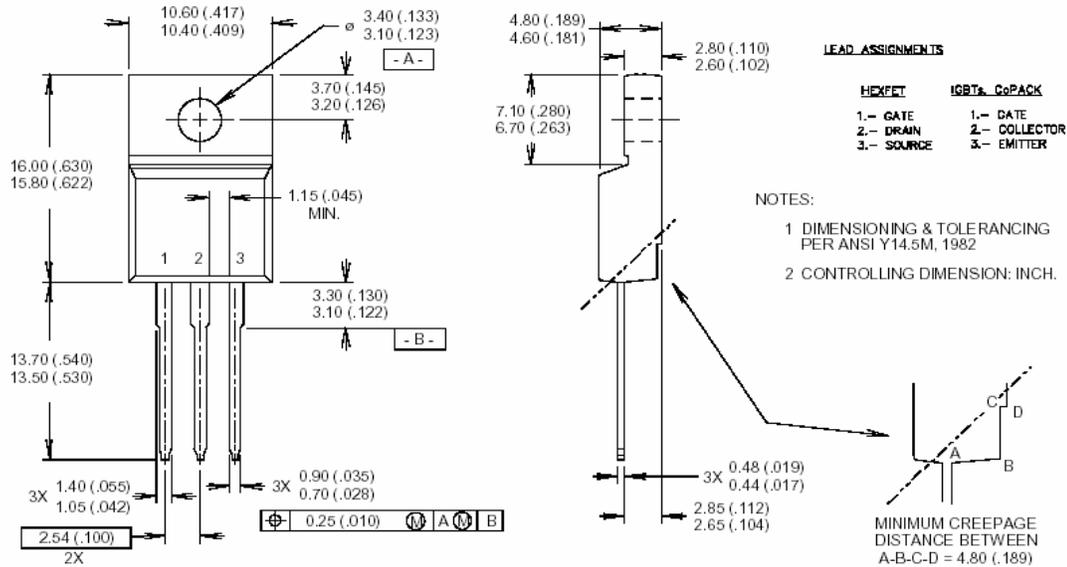
TO-220 Full-Pak Part Marking Information

EXAMPLE: THIS IS AN IRFI840G
WITH ASSEMBLY
LOT CODE 3432
ASSEMBLED ON WW 24 1999
IN THE ASSEMBLY LINE "K"

INTERNATIONAL RECTIFIER LOGO

ASSEMBLY LOT CODE

PART NUMBER

DATE CODE
YEAR 9 = 1999
WEEK 24
LINE K
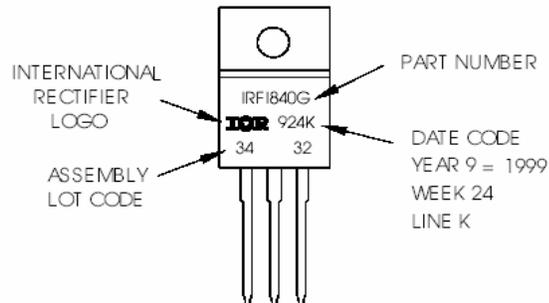
TO-220 Full-Pak package is not recommended for Surface Mount Application

Data and specifications subject to change without notice.
This product has been designed and qualified for the Industrial market.
Qualification Standards can be found on IR's Web site.

International IGR Rectifier